

# Induced Furoeudesmanes: A Defense Mechanism Against Stress in *Laggera pterodonta*, a Chinese Herbal Plant

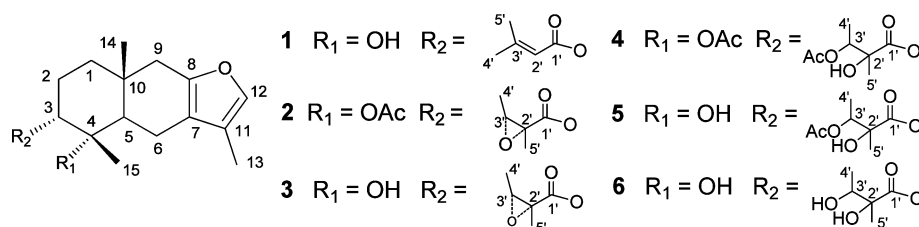
Ya-Ping Liu,<sup>†</sup> Ren Lai,<sup>‡</sup> Yong-Gang Yao,<sup>‡</sup> Zhong-Kai Zhang,<sup>§</sup> En-Tang Pu,<sup>§</sup> Xiang-Hai Cai,<sup>†</sup> and Xiao-Dong Luo<sup>\*†</sup>

State Key Laboratory of Phytochemistry and Plant Resources in West China, Kunming Institute of Botany, Chinese Academy of Sciences, Kunming 650204, People's Republic of China, Key Laboratory of Animal Models and Human Disease Mechanisms, Kunming Institute of Zoology, Chinese Academy of Sciences, Kunming 650223, People's Republic of China, and Yunnan Academy of Agricultural Sciences, Kunming 650205, People's Republic of China

xdluo@mail.kib.ac.cn

Received July 29, 2013

## ABSTRACT



*Laggera pterodonta* displays different phenotypes in its natural habitat but expresses a uniform phenotype with large, broad leaves and fewer secondary metabolites when grown under optimal conditions. The production of six furoeudesmanes is only induced when *L. pterodonta* encounters stresses, conferring host resistance against a broad spectrum of plant invaders.

Plant secondary metabolites are compounds present in specialized cells that are not essential for cellular metabolism yet are required for the survival of the plant within its external environment.<sup>1</sup> These compounds are believed to assist plant defense against insect herbivory and pathogenic attack.<sup>2</sup> Plants have played a dominant role in traditional medicine systems, and the importance of secondary small molecular compounds in plants is significant to pharmacognosy and the development of synthetic derivatives for the pharmaceutical industry. However, these compounds did not undergo their evolutionary selection based on human therapeutic agents, rather environmental defensive systems, but what causes plants to synthesize many different secondary metabolites remains largely unexplored. Therefore, the research into the causes of the induction of these downstream compounds, their

structure, and the role they perform in plants is attracting a lot of attention from chemists and physiologists.

*Laggera pterodonta* is widely distributed in Southwest China and has been used historically in the “Yi” ethnopharmacy as an anti-inflammatory and antibacterial agent.<sup>3</sup> Previous investigations reported the isolation of flavonoids and eudesmanes from this plant.<sup>4</sup> In our pharmacological evaluation test, the main sesquiterpenoid, pterodonic acid (PA),<sup>4d</sup> was shown to have an anti-inflammatory effect as observed by decreasing xylene-induced ear edema in mice by up to 64.1% at a dosage of 10 mg/kg, roughly comparable to that of aspirin at 200 mg/kg (73.7%) (Supporting Information, Table S1).

(3) Jiangsu New Medical College. *A Dictionary of Chinese Traditional Medicine*; Shanghai Science and Technology Press: Shanghai, 1977.

(4) (a) Zhao, Y.; Yue, J. M.; Sun, H. D. *Acta Botanica Yunnanica* **1997**, *19*, 207–210. (b) Li, S. L.; Ding, J. K. *Acta Botanica Yunnanica* **1993**, *15*, 303–305. (c) Li, S. L.; Ding, J. K. *Acta Botanica Yunnanica* **1994**, *16*, 313–314. (d) Li, S. L.; Ding, J. K. *Acta Botanica Yunnanica* **1996**, *18*, 349–352. (e) Li, S. L.; Ding, J. K. *Acta Botanica Yunnanica* **1994**, *16*, 434–436.

<sup>†</sup> Kunming Institute of Botany.

<sup>‡</sup> Kunming Institute of Zoology.

<sup>§</sup> Yunnan Academy of Agricultural Sciences.

(1) Sultan, S. E. *Curr. Opin. Plant Biol.* **2010**, *13*, 96–101.

(2) Kliebenstein, D. J. *Plant Cell Environ.* **2004**, *27*, 675–684.

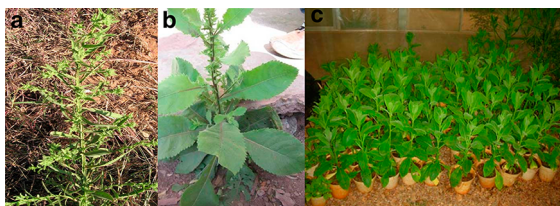


**Figure 1.** Different phenotypes of *L. pterodonta*. (a) *L. pterodonta* grown in dry soil had multiple branches and narrow leaves. (b) *L. pterodonta* produced fewer branches and large broad leaves when grown in moist conditions. (c) Same phenotype of *L. pterodonta* was cultivated in a greenhouse from the seeds of the different phenotypes.

During the medicine quality control procedure, we did not find any PA in some preparations, which led to the discovery that two phenotypes of *L. pterodonta* (Figure 1a,b) exist in the wild. Both phenotypes of this plant have been used as the raw material for herbal medicines, but the plants with broad leaves did not produce PA. This finding led us to question the basis for the phenotype. Next, we collected seeds of *L. pterodonta* with different phenotypes and cultivated them in a greenhouse under optimal conditions, such as abundant moisture (50–60% RH) and appropriate temperature (25 °C). Intriguingly, all the plants grew with large broad leaves, produced fewer secondary metabolites, and became sensitive to insect attack (Figure 1c). Surprisingly, after 3 days of continual attack by insect larvae (*Neurois renalba* or *Argyrogramma agnate*), the six compounds were induced in the leaves of plants. However, after 10 days, these induced compounds gradually decreased in concentration, possibly via degradation.

After grinding leaf tissue with their mandibles, insects (larvae) use oral secretions to transport food into their mouthparts. These oral secretions, composed of regurgitant labial and mandibular saliva, contain a mixture of potential elicitors that are recognized by the plant, which produce a defense response.<sup>5</sup> To determine whether the biosynthesis of the six compounds were triggered by the oral secretion of insect herbivory or simply caused by wounding,<sup>6</sup> we prepared *L. pterodonta* in tissue culture seedlings in an incubator and cultivated the plants in a greenhouse. Plants were divided randomly and maintained separately. Chafing and cutting were used to cause wounding (Figure 2a). Our results showed that the six compounds were induced in the leaves of all the wounded plants, and their concentrations were observed to be proportional to the degree of wounding (Figure 2b and Supporting Information).

Previous studies showed that the plants defended themselves against insect herbivory attack using chemical and physiological defenses by synthesizing and rapidly releasing volatile organic compounds (VOCs). Subsequently, adjacent plants detected the VOCs released by the

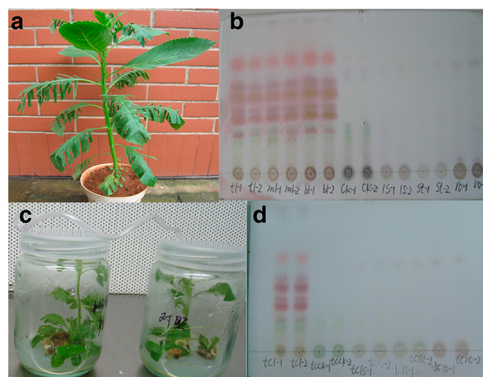


**Figure 2.** Inducible compounds in *L. pterodonta*. (a) Cut plant. (b) Thin layer chromatogram (TLC) profile showed that all leaves of the treated plant produced six induced compounds (red spots, lanes 1–6), whereas its leafstalk (lanes 9 and 10), stem (lanes 11 and 12), root (lanes 13 and 14), and leaves of the unwounded plant (lanes 7 and 8) did not. (c) Two culture flasks linked by polyvinyl chloride pipe; the seedling of *L. pterodonta* on the left flask was cut, while the plant was kept intact in the right flask. (d) TLC profile of *L. pterodonta* in both flasks showed the presence of induced compounds in leaves (red spots, lanes 1 and 2), but not in leafstalk (lanes 5 and 6), stem (lanes 7 and 8), root (lanes 9 and 10), and control (lanes 3 and 4).

neighboring wounded plants and then activated their own defenses before being attacked.<sup>7</sup> To demonstrate this association, we developed apparatus that permitted the transmission of volatile compounds from one plant to another (Figure 2c). Seedlings of *L. pterodonta* were cut in one flask, while the intact plants were growing in the connected flask. Intriguingly, we found that the six compounds were detectable in the undamaged plants, in approximately equivalent proportions to those of the wounded plants (Figure 2d).

It is well-established that jasmonate (JA) plays a prominent role in promoting plant defense responses to herbivores and wounding, while salicylic acid (SA) crucial for the plant's defense is generally involved in the establishment of systemic acquired resistance. Unlike protease inhibitor (PI) induced by JA and pathogenesis-related (PR) proteins induced by SA, plant secondary metabolite defense was related to the downstream products of stress signals.<sup>8</sup> However, are these induced compounds specific to the JA pathway or related to stress phytohormones? In order to test this hypothesis, we treated both cultivated plants in a greenhouse and tissue culture seedlings of *L. pterodonta*, with signal molecules of wounding (JA), pathogens (SA), and induced drought (abscisic acid and ethrel), respectively, to mimic environmental stresses (Supporting Information). Surprisingly, the six induced compounds were detected in the leaves of all the treated plants but not in the controls. Furthermore, high temperature (> 40 °C), low temperature (< 5 °C), and intense

(5) Weech, M. H.; Chapleau, M.; Pan, L.; Ide, C.; Bede, J. C. *J. Exp. Bot.* **2008**, *59*, 2437–2448.

(6) Alborn, H. T.; Turlings, T. C. J.; Jones, T. H.; Stenhagen, G.; Loughrin, J. H.; Tumlinson, J. H. *Science* **1997**, *276*, 945–949.

(7) (a) Baldwin, I. T.; Halitschke, R.; Paschold, A.; Dahl, C. C. V.; Preston, C. A. *Science* **2006**, *311*, 812–815. (b) Moraes, C. M. D.; Mescher, M. C.; Tumlinson, J. H. *Nature* **2001**, *410*, 577–580.

(8) (a) Bari, R.; Jones, J. D. G. *Plant Mol. Biol.* **2009**, *69*, 473–488. (b) Grant, H. S.; Jones, J. H. *Anal. Chem.* **1950**, *22*, 679–681.

ultraviolet (1200 lux, 5 h) conditions could also induce the biosynthesis of these compounds in tissue culture seedlings. Evidently, the biosynthesis of these compounds was in response to a variety of stimuli.

The six induced compounds (red spots on TLC) were isolated by rapid column chromatography repeatedly at low temperature (to avoid decomposition), and they were elucidated to be furoeudesmanes by detailed analysis of their spectral data and X-ray; of which **1**, **2**, and **4–6** were novel (Figures S1 and S4–S38, Tables S2 and S3).

Compound **3** was determined to be 3 $\alpha$ -(2',3'-epoxy-2'-methylbutyryloxy)furoepaltol by comparison of its <sup>1</sup>H and <sup>13</sup>C NMR data with the literature.<sup>9</sup> Single-crystal X-ray diffraction further supported the structure and clarified the relative configuration of **3** (Figure S1 and Supporting Information). The <sup>1</sup>H and <sup>13</sup>C NMR spectra of **1**<sup>10</sup> were similar to those of **3**, except for the substituent group at C-3. Two methyl protons appeared as singlets at  $\delta_{\text{H}}$  1.86 and 2.14, together with an olefinic proton at  $\delta_{\text{H}}$  5.76 (s), and corresponding carbon signals at  $\delta_{\text{C}}$  117.3 (d) and 156.7 (s) in **1** suggested a 2'(3')-ene-3'-methylbutyryloxy as the substituent,<sup>9</sup> which was in accord with its molecular formula of C<sub>20</sub>H<sub>28</sub>O<sub>4</sub>. The HMBC correlation of  $\delta_{\text{H}}$  4.80 (m, H-3) with  $\delta_{\text{C}}$  166.3 (C-1', s) further supported the substituent at C-3.

Comparison of <sup>1</sup>H and <sup>13</sup>C NMR data of **2**<sup>11</sup> with those of **3** suggested one more acetyl group in **2**. The HMBC correlation of  $\delta_{\text{H}}$  1.95 (3H, s) with a quaternary carbon at  $\delta_{\text{C}}$  83.9 (C-4) suggested the acetylation of 4-OH.

The <sup>1</sup>H and <sup>13</sup>C NMR spectra of **4**<sup>12</sup> were very similar to those of **2**, except for a pair of downfield signals at  $\delta_{\text{C}}$  75.8 (s), 74.4 (d) in **4** instead of  $\delta_{\text{C}}$  60.3 (s), 59.8 (d) in **2**, which suggested the cleavage of an epoxy group at the substituent. An additional acetyl group ( $\delta_{\text{C}}$  20.1, q and 169.9, s) was connected to 3'-OH, revealed by the downfield signal at  $\delta_{\text{H}}$  5.03 (q,  $J = 6.3$  Hz, H-3'), which was further supported by the HMBC correlation of  $\delta_{\text{H}}$  1.98 (3H, s) with  $\delta_{\text{C}}$  74.4 (d, C-3').

The <sup>1</sup>H and <sup>13</sup>C NMR spectra of **5**<sup>13</sup> displayed similarity to those of **4** except for the presence of only one acetyl group in **5**, in accordance with its molecular formula of C<sub>22</sub>H<sub>32</sub>O<sub>7</sub>. The acetyl group was connected to 3'-OH, supported by the HMBC correlation of downfield proton H-3' ( $\delta_{\text{H}}$  5.10, q,  $J = 6.3$  Hz) with  $\delta_{\text{C}}$  170.2 (s).

(9) Zdero, C.; Bohlmann, F. *Phytochemistry* **1989**, *28*, 3097–3100.

(10) Compound **1**: white oil; TLC (petroleum ether/Me<sub>2</sub>CO, 3:1 v/v);  $R_f = 0.55$ ; IR (film)  $\nu_{\text{max}}$  3499, 2925, 1716, 1233, 1082 cm<sup>-1</sup>; <sup>1</sup>H and <sup>13</sup>C NMR data, see Tables S2 and S3, respectively; HRESIMS ( $m/z$ ) [M + H]<sup>+</sup> calcd for C<sub>20</sub>H<sub>28</sub>O<sub>4</sub> 333.2065, found 333.2074.

(11) Compound **2**: colorless oil; TLC (petroleum ether/Me<sub>2</sub>CO, 3:1 v/v);  $R_f = 0.47$ ; IR (film)  $\nu_{\text{max}}$  2933, 1752, 1247, 1143 cm<sup>-1</sup>; <sup>1</sup>H and <sup>13</sup>C NMR data, see Tables S2 and S3, respectively; HRESIMS ( $m/z$ ) [M + Na]<sup>+</sup> calcd for C<sub>22</sub>H<sub>30</sub>O<sub>6</sub>Na 413.1940, found 413.1927.

(12) Compound **4**: white amorphous powder; TLC (petroleum ether/Me<sub>2</sub>CO, 3:1 v/v);  $R_f = 0.38$ ; IR (KBr)  $\nu_{\text{max}}$  3441, 2942, 1739, 1245, 1065 cm<sup>-1</sup>; <sup>1</sup>H and <sup>13</sup>C NMR data, see Tables S2 and S3, respectively; HRESIMS ( $m/z$ ) [M + H]<sup>+</sup> calcd for C<sub>24</sub>H<sub>35</sub>O<sub>8</sub> 451.2331, found 451.2340.

(13) Compound **5**: white amorphous powder; TLC (petroleum ether/Me<sub>2</sub>CO, 3:1 v/v);  $R_f = 0.33$ ; IR (KBr)  $\nu_{\text{max}}$  3503, 2938, 1742, 1254, 1067 cm<sup>-1</sup>; <sup>1</sup>H and <sup>13</sup>C NMR data, see Tables S2 and S3, respectively; HRESIMS ( $m/z$ ) [M + H]<sup>+</sup> calcd for C<sub>22</sub>H<sub>33</sub>O<sub>7</sub> 409.2226, found 409.2213.

**Table 1.** Antifeeding Activity of the Induced Furoeudesmanes Against the Larvae of Four Species of Insects<sup>a</sup>

compounds	<i>A. agnate</i>	<i>S. exigua</i>	<i>P. rapae</i>	<i>P. xylostella</i>
<b>1</b>	83.5 ± 3.7	59.1 ± 4.8	42.6 ± 3.6	39.5 ± 3.2
<b>2</b>	92.4 ± 4.6	82.8 ± 2.4	63.4 ± 3.2	31.8 ± 2.3
<b>3</b>	90.5 ± 3.9	80.9 ± 4.0	44.9 ± 1.5	39.4 ± 4.6
<b>4</b>	96.5 ± 3.1	48.7 ± 3.6	52.2 ± 3.3	28.6 ± 3.7
<b>5</b>	86.8 ± 5.8	90.3 ± 1.7	72.6 ± 2.5	27.4 ± 3.5
<b>6</b>	76.7 ± 1.6	51.1 ± 3.7	59.9 ± 4.0	35.4 ± 2.4
azadirachtin	94.6 ± 3.8	89.7 ± 2.4	76.8 ± 3.1	46.6 ± 1.9

<sup>a</sup>The tested concentrations were 20  $\mu\text{g}$ /leaf-disk, equal to 0.80  $\mu\text{g}$ /mg fresh cabbage leaves. All values are expressed as mean ± SE for all groups ( $n = 3$ ).

**Table 2.** Inhibitory Constants of the Induced Furoeudesmanes to Hydrolysis of Synthetic Chromogenic Substrates<sup>a</sup>

compounds	inhibitory constant ( $K_i$ )	
	serine protease of <i>Pieris rapae</i>	serine protease of <i>Drosophila melanogaster</i>
<b>1</b>	$4.28 \times 10^{-5}$	$3.76 \times 10^{-5}$
<b>2</b>	$2.99 \times 10^{-5}$	$3.27 \times 10^{-5}$
<b>3</b>	$6.17 \times 10^{-5}$	$4.38 \times 10^{-5}$
<b>4</b>	$2.00 \times 10^{-4}$	$8.67 \times 10^{-5}$
<b>5</b>	$8.75 \times 10^{-4}$	$7.48 \times 10^{-5}$
<b>6</b>	$2.69 \times 10^{-5}$	$5.50 \times 10^{-5}$
azadirachtin	$2.88 \times 10^{-5}$	$3.25 \times 10^{-5}$

<sup>a</sup>The concentrations of compounds were 100  $\mu\text{g}$ /mL. All results are expressed as mean ± SE for all groups ( $n = 3$ ).

Compound **6**<sup>14</sup> was shown to be a deacetylated derivative of **5** by detailed comparison of <sup>1</sup>H and <sup>13</sup>C NMR spectra of two compounds, in accordance with its molecular formula of C<sub>20</sub>H<sub>30</sub>O<sub>6</sub>.

Observation under greenhouse conditions and the disk test revealed that the larvae of *N. renalba* preferred leaves of *L. pterodonta* without the induced compounds (Figure S3). An antifeeding evaluation of the induced furoeudesmanes was also performed against the second-instar larvae of *Argyrogramma agnate*, *Spodoptera exigua*, *Pieris rapae*, and the third-instar larvae of *Plutella xylostella*, by using the conventional leaf-disk method (Supporting Information). All six compounds showed significant antifeeding activities, in which compounds **2**, **3**, and **5** displayed an approximately equal effect to the well-known antifeedant, azadirachtin (Table 1). Specifically, the induced compounds inhibit the digestion of plant proteins by the insects, as suggested by the result of the serine protease (from the midgut of the larvae) inhibition assay (Table 2).

During our 5 year observation, we have not seen any *L. pterodonta* plants that have been infected by pathogens

(14) Compound **6**: white amorphous powder; TLC (petroleum ether/Me<sub>2</sub>CO, 3:1 v/v);  $R_f = 0.25$ ; IR (KBr)  $\nu_{\text{max}}$  3441, 2938, 1773, 1247, 1270 cm<sup>-1</sup>; <sup>1</sup>H and <sup>13</sup>C NMR data, see Tables S2 and S3, respectively; HRESIMS ( $m/z$ ) [M + H]<sup>+</sup> calcd for C<sub>20</sub>H<sub>31</sub>O<sub>6</sub> 367.2120, found 367.2122.

**Table 3.** TMV Infection Inhibition Activities of the Induced Furoeudesmanes on *N. glutinosa*<sup>a</sup>

compounds	inhibition rate (%)	compounds	inhibition rate (%)
<b>1</b>	52.9 ± 2.1	<b>5</b>	43.1 ± 2.2
<b>2</b>	50.8 ± 2.6	<b>6</b>	58.1 ± 3.4
<b>3</b>	44.3 ± 1.6	ningnanmycin	58.6 ± 2.0
<b>4</b>	39.9 ± 2.1		

<sup>a</sup> The concentrations of compounds ranged from 0.01 to 10 μM.

in the wild or in our greenhouse. Furthermore, plants were infected by artificial inoculation with common agricultural pathogens. Tobacco mosaic virus (TMV), one of the most well-studied plant viruses, infecting more than 400 plant species that belong to 36 families,<sup>15</sup> was selected to evaluate the antiviral activity of the six induced furoeudesmanes from *L. pterodonta*. These induced compounds exhibited a marked inhibition activity against TMV replication at the local lesion host in *Nicotiana glutinosa* by the half-leaf method, comparable to ningnanmycin (Table 3 and Supporting Information).

The leaf-disk method was also used to evaluate the inhibition of the induced furoeudesmanes on TMV replication in the systemic infection host, *N. tabacum* cv.K326. The concentration of TMV was assayed by triple antibody sandwich ELISA (TAS-ELISA), and the accumulation of TMV coat protein (CP) was tested by Western blot analysis (Figure 3 and Supporting Information). The result showed that all the compounds inhibited TMV replication, with compounds **1**, **2**, and **6** reducing the accumulation of the TMV CP significantly (Figure 3).

The concentrations of six compounds are proportional to the degree of wounding and decomposition. To further quantify the concentrations of compounds, samples were analyzed by HPLC, and we found that their contents could reach a maxima of 0.23% (**1**), 0.20% (**2**), 0.43% (**3**), 0.081% (**4**), 0.27% (**5**), and 0.16% (**6**) in fresh leaf, respectively (Figure S2). These concentrations were apparently higher than those needed to prevent the antifeeding and antivirus effects (Tables 1–3).

Our observation that *L. pterodonta* with large broad leaves produces fewer secondary metabolites when grown in optimal conditions provides a suitable model to understand the important balance between the allocation of energy for growth and secondary metabolites required for the synthesis of defense molecules. The biosynthesis of the six induced furoeudesmanes in *L. pterodonta* was not triggered until the plant encountered one of many stimuli.

(15) (a) Craeger, A. N.; Scholthof, K. B.; Citovsky, V.; Scholthof, H. B. *Plant Cell* **1999**, *11*, 301–308. (b) Ritzenthaler, C. *Curr. Opin. Biotechnol.* **2005**, *16*, 118–122. (c) Liu, L. R. *The Control of Disease and Pest of Tobacco*; Science Press: Beijing, 1998.

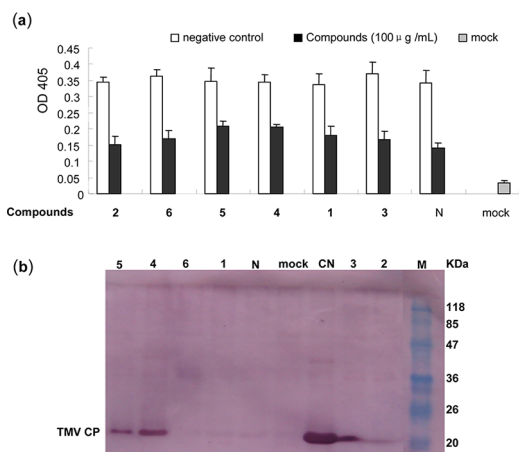


**Figure 3.** Inhibitory effects of compounds **1–6** (100 μg/mL) against TMV replication in *N. tabacum* cv.K326. (a) Replication of TMV was determined by TAS-ELISA. All results are expressed as mean ± SE ( $n = 3$ ). (b) TMV coat protein (CP) was measured by Western blot. Lane M refers to protein marker; lane N refers to treatment with ningnanmycin (100 μg/mL); lane CN means control; other lanes refer to treatment with the six compounds, respectively.

However, these secondary metabolites have a role to assist the plant to confer host resistance against insects and viruses. In this way, the induction of secondary metabolites could perform a nonspecific and secondary defensive role in augmenting other well-known responses, such as the systemic wound response and systemic acquired resistance. Additionally, our finding suggests that favorable conditions for plant growth may not be good for the accumulation of the secondary metabolites in the production of medicinal plants.

**Acknowledgment.** The authors are grateful to the National Natural Science Foundation of China (81225024), the Chinese Academy of Science (*XiBuZhiGuang* project) and State Key Laboratory of Phytochemistry (P2008-ZZ15) for partial financial support. The authors thank Ian Logan (Biologist, Exmouth, Devon, UK) and Simon Cichello (English editor of *Natural Products & Bioprospecting*, Melbourne, Australia) for helpful comments and language editing.

**Supporting Information Available.** Supplementary text, Figures S1–S38, Tables S1–S3, refs S1–S12, and X-ray crystallographic data (CIF file) of compound **3**. This material is available free of charge via the Internet at <http://pubs.acs.org>.

The authors declare no competing financial interest.

Supplementary Information for  
Induced Furoeudesmanes: A Defense Mechanism Against Stress  
in *Laggera pterodonta*, a Chinese Herbal Plant

*Ya-Ping Liu, Ren Lai, Yong-Gang Yao, Zhong-Kai Zhang, En-Tang Pu, Xiang-Hai Cai, Xiao-Dong Luo\**

\*To whom correspondence should be addressed. E-mail: xdluo@mail.kib.ac.cn.

**This PDF file includes:**

Supplementary Text

S1. Materials and Methods of Induced Furoeudesmanes

S1.1. Plant material and growing conditions

S1.2. Tissue culture and growing conditions

S1.3. Induction of furoeudesmanes by the signal molecules

S2. Structure Elucidation of Induced Furoeudesmanes and Quantitative Analysis

S2.1. Spectroscopic methods

S2.2. Extraction and Isolation of the induced compounds

S2.3. Structure elucidation of the induced compounds

S2.4. Quantitative HPLC-PDA analysis

S3. Biological Activity Assay of Induced Furoeudesmanes

S3.1. Anti-inflammatory evaluation: xylene-induced ear edema in mice

S3.2. Insecticidal Assay

S3.3. Anti-tobacco mosaic virus (TMV) assays

Figures S1 to S38.

Tables S1 to S3.

References S1 to S12.

## Supplementary Text

### S1. Materials and Methods of Induced Furoeudesmanes

#### S1.1 Plant material and growing conditions

*Laggera pterodonta* is widely distributed in Southwest of China, and seeds of *L. pterodonta* with different phenotypes were collected during November and December each year from plants growing in their original habitats. The seeds were germinated in Petri dishes on moistened filter papers and bare-root seedlings were transplanted into pots after 2 weeks. All the plants were cultivated in a greenhouse which was set at a constant temperature of 25°C, with a 16:8 L: D light cycle, at the Kunming Institute of Botany, Chinese Academy of Sciences. Plants were watered regularly and allowed to grow for 12 weeks.

#### S1.2. Tissue culture and growing conditions

The shoot tips of *L. pterodonta* were used as explants to set up the non-bacillus propagation system through induction, proliferation, rooting culture and transplantation. The shoot tips for tissue cultures were taken to the laboratory and rinsed with cold water for an hour. And then surface-sterilized for 0.5 min in 75% (v/v) ethanol and rinsed three times with sterile, deionized water, followed by a treatment with 0.1% (v/v) HgCl<sub>2</sub> for 1 min, and rinsed five times with deionized water.<sup>S1</sup> Subsequently, the surface-sterilized explants were spread on induction medium: Murashige-Skoog (MS) medium<sup>S2</sup> supplemented with 2.0 mg/L of 6-benzylaminopurine (6-BA) and 0.5 mg/L of  $\alpha$ -naphthylacetic acid (NAA). Cultures were preincubated at 25°C in the dark for 2 weeks, and then were cultivated in a proliferation medium (MS basal medium containing 4.0 mg/L of 6-BA and 0.5 mg/L of NAA) at 25°C with 16 h/d photoperiod for 3 weeks, finally transferred to a rooting medium (1/2MS basal medium adding 0.2 mg/L of NAA) at 25°C with 16 h/d photoperiod for 6 weeks, to prepare tissue culture seedlings for the experiments. All media were solidified with agar at 7.5 g/L and adjusted to pH 5.6-5.8 with NaOH, then autoclaved for 20 min at 121°C and 1.1 kg/cm<sup>2</sup> pressure.

#### S1.3. Induction of furoeudesmanes by the signal molecules

The signal molecules of wounding (JA), pathogens (SA) and drought (abscisic acid

[ABA] and Ethene) were applied to mimic environmental stresses. The signal molecules were dissolved in 0.5 mL DMSO and diluted with distilled H<sub>2</sub>O. The final concentrations were 300  $\mu\text{g/L}$  of JA, SA, ABA, and Ethene to each 12 weeks-old *L. pterodonta* in the green-house, and 100  $\mu\text{g/L}$  of sterilized JA, SA, ABA, and Ethene to tissue culture seedlings (6 weeks-old) in the incubator, respectively. Each treatment group contained three separate plants, and all experiments were replicated at least three times. Six induced furoeudesmanes were detectable in all the leaves of the treated plants after 3 days of treatment, but absent from the control plants.

## S2. Structure Elucidation of Induced Furoeudesmanes and Quantitative Analysis

### S2.1. Spectroscopic methods

Nuclear magnetic resonance (NMR) spectra were run on a Bruker DRX-500 spectrometer with TMS as an internal standard. Chemical shifts ( $\delta$ ) were expressed in ppm with reference to the solvent signals. X-ray diffraction was performed using a Bruker SMART APEX CCD crystallography system. Infrared (IR) spectra were obtained with a Tenor 27 spectrophotometer using KBr pellets or film. Electrode spray ionization mass spectra (ESI-MS) were obtained on an API QSTAR Pulsar I spectrometer. Column chromatography (CC) was performed on silica gel (200-300 mesh, Qingdao Marine Chemical Ltd., Qingdao, China), reverse phase C-18 (RP-18) silica gel (20-45  $\mu\text{m}$ , Fuji Silysia Chemical Ltd., Japan), and Sephadex LH-20 (Pharmacia Fine Chemical Co., Ltd., Sweden). Fractions were monitored by using a thin layer chromatogram (TLC) (GF 254, Qingdao Marine Chemical Ltd., Qingdao, China), and spots were visualized by heating silica gel plates sprayed with 10% H<sub>2</sub>SO<sub>4</sub> and 0.01% anisaldehyde in EtOH. HPLC analyses were performed on a Waters Alliance 2695 and monitored by a Waters 2996 photodiode array detector (PDA) scanning device from 200 to 600 nm.

### S2.2. Extraction and Isolation of the induced compounds

For the induced compounds do decompose very easily during extraction and isolation, all of the procedures must be conducted at low temperature, and the samples were stored in a refrigerator. The fresh leaves of the induced *L. Pterodonta* (1.5 kg) were crushed and extracted with acetone (8 h  $\times$  1). The acetone extracts were evaporated *in vacuo* to give the viscous residue extract, which was partitioned with petroleum ether to afford petroleum ether and H<sub>2</sub>O layers.

The petroleum ether fraction (8.5 g) was subjected to middle-performance liquid chromatography (MPLC) with RP-18, using the MeOH-H<sub>2</sub>O (from 5:5 to 9:1) to produce fractions I-V. Fraction II (2.36 g) was separated by MPLC with RP-18 CC (MeOH-H<sub>2</sub>O, 50:50, 55:45, 60:40) to give subfractions A-C. Subfraction B was further purified by Sephadex LH-20 CC (MeOH), and then by silica gel CC (petroleum ether-Me<sub>2</sub>CO, 10:1 and 8:1) to yield **6** (48 mg) and **5** (71 mg). Separation of fraction III (1.6 g) by RP-18 CC, eluted with MeOH-H<sub>2</sub>O (55:45, 60:40, 65:35, 70:30) repeatedly, and then by Sephadex LH-20 CC (MeOH) to give **4** (87 mg) and **3** (115 mg). Fraction IV (840 mg) was applied on RP-18 CC using MeOH-H<sub>2</sub>O (70:30, 75:25, 80:20) and then chromatographed on a silica gel CC (petroleum ether- Me<sub>2</sub>CO, 30:1 and 20:1) to give **2** (45 mg) and **1** (30 mg).

### S2.3. Structure elucidation of the induced compounds

Six compounds were isolated by rapid column chromatography repeatedly at low temperature (to avoid decomposition) and were elucidated as furoeudesmanes by detailed analysis of their spectra and X-ray data. Compounds **1**, **2**, and **4–6** were found to be new. All signals for compounds **1–6** were assigned in Tables S2 and S3 on the basis of the 2D NMR spectral data.

Compound **3** was determined to be 3 $\alpha$ -(2',3'-epoxy-2'-methylbutyryloxy)-furoepaltol by comparison of its <sup>1</sup>H and <sup>13</sup>C NMR data with that given in the published literature. Single crystal X-ray diffraction further confirm the structure and clarified the relative configuration of **3** (Figure S1). The <sup>1</sup>H and <sup>13</sup>C NMR spectra of **1** were similar to those of **3**, except for the substituent group at C-3. Two methyl protons appeared as singlet at  $\delta_{\text{H}}$  1.86 and 2.14, together with an olefinic proton at  $\delta_{\text{H}}$  5.76 (s) and corresponding carbon signals at  $\delta_{\text{C}}$  117.3 (d) and 156.7 (s) in **1** suggested a 2'(3')-ene-3'-methylbutyryloxy as substituent, which was accordant to its molecular formula of C<sub>20</sub>H<sub>28</sub>O<sub>4</sub>. The HMBC correlation of  $\delta_{\text{H}}$  4.80 (m, H-3) with  $\delta_{\text{C}}$  166.3 (C-1', s) positioned the substituent at C-3. Comparison of <sup>1</sup>H and <sup>13</sup>C NMR data of **2** with those of **3** suggested one more acetyl in **2**. The HMBC correlation of  $\delta_{\text{H}}$  1.95 (3H, s) with a downfield quaternary carbon at  $\delta_{\text{C}}$  83.9 (C-4) suggested the acetylation of 4-OH.

The <sup>1</sup>H and <sup>13</sup>C NMR spectra of **4** were very similar to those of **2**, except for a pair of downfield signals at  $\delta_{\text{C}}$  75.8 (s), 74.4 (d) in **4** instead of  $\delta_{\text{C}}$  60.3 (s), 59.8 (d) in **2**, which

suggested the cleavage of an epoxy group substituent. An additional acetyl group ( $\delta_C$  20.1, q and 169.9, s) was connected to 3'-OH, as suggested by the downfield signal at  $\delta_H$  5.03 (q,  $J = 6.3$  Hz, H-3'), which was further supported by the HMBC correlations of  $\delta_H$  1.98 (3H, s) with  $\delta_C$  74.4 (d, C-3'). The  $^1H$  and  $^{13}C$  NMR spectra of **5** displayed similarity to those of **4** with the exception of only one acetyl group in **5**, in accordance with its molecular formula of  $C_{22}H_{32}O_7$ . The acetyl group was connected to 3'-OH, supported by the HMBC correlations of downfield proton H-3' ( $\delta_H$  5.10, q,  $J = 6.3$  Hz) with  $\delta_C$  170.2 (s). Compound **6** was elucidated to be a deacetylated derivative of **5** by detailed comparison of  $^1H$  and  $^{13}C$ -NMR spectra of the two compounds, in accordance with its molecular formula of  $C_{20}H_{30}O_6$ .

$3\alpha$ -(2'(3')-ene-3'-methylbutyryloxy)-furoepaltol (**1**). White oil; TLC (petroleum ether/ $Me_2CO$ , 3:1 v/v):  $R_f = 0.55$ ;  $^1H$  NMR ( $Me_2CO$ , 500 MHz) see Table S2,  $^{13}C$  NMR ( $Me_2CO$ , 125 MHz) see Table S3, IR (film)  $\nu_{max}$  3499, 2925, 1716, 1233, 1082  $cm^{-1}$ ; HRESIMS ( $m/z$ )  $[M+H]^+$  calcd for  $C_{20}H_{29}O_4$ , 333.2065; found 333.2074.

$3\alpha$ -(2 $\alpha'$ ,3 $\alpha'$ -epoxy-2'-methylbutyryloxy)-4 $\alpha$ -acetyfuroepaltol (**2**). Colorless oil; TLC (petroleum ether/ $Me_2CO$ , 3:1 v/v):  $R_f = 0.47$ ;  $^1H$  NMR ( $Me_2CO$ , 500 MHz) see Table S2,  $^{13}C$  NMR ( $Me_2CO$ , 125 MHz) see Table S3, IR (film)  $\nu_{max}$  2933, 1752, 1247, 1143  $cm^{-1}$ ; HRESIMS ( $m/z$ )  $[M+Na]^+$  calcd for  $C_{22}H_{30}O_6Na$ , 413.1940; found 413.1927.

$3\alpha$ -(2 $\alpha'$ ,3 $\alpha'$ -epoxy-2'-methylbutyryloxy)-furoepaltol (**3**). White crystal ( $MeOH$  and  $H_2O$ ); TLC (petroleum ether/ $Me_2CO$ , 3:1 v/v):  $R_f = 0.41$ ;  $^1H$  NMR ( $Me_2CO$ , 500 MHz) see Table S2,  $^{13}C$  NMR ( $Me_2CO$ , 125 MHz) see Table S3.

$3\alpha$ -(2'-hydroxy-2'-methyl-3'-acetoxybutyryloxy)-4 $\alpha$ -acetyfuroepaltol (**4**). White amorphous powder; TLC (petroleum ether/ $Me_2CO$ , 3:1 v/v):  $R_f = 0.38$ ;  $^1H$  NMR ( $Me_2CO$ , 500 MHz) see Table S2,  $^{13}C$  NMR ( $Me_2CO$ , 125 MHz) see Table S3, IR (KBr)  $\nu_{max}$  3441, 2942, 1739, 1245, 1065  $cm^{-1}$ ; HRESIMS ( $m/z$ )  $[M+H]^+$  calcd for  $C_{24}H_{35}O_8$ , 451.2331; found 451.2340.

$3\alpha$ -(2'-hydroxy-2'-methyl-3'-acetoxybutyryloxy)-furoepaltol (**5**). White amorphous powder; TLC (petroleum ether/ $Me_2CO$ , 3:1 v/v):  $R_f = 0.33$ ;  $^1H$  NMR ( $Me_2CO$ , 500 MHz) see Table S2,  $^{13}C$  NMR ( $Me_2CO$ , 125 MHz) see Table S3, IR (KBr)  $\nu_{max}$  3503, 2938, 1742, 1254, 1067  $cm^{-1}$ ; HRESIMS ( $m/z$ )  $[M+H]^+$  calcd for  $C_{22}H_{33}O_7$ , 409.2226; found 409.2213.

3 $\alpha$ -(2',3'-dihydroxy-2'-methylbutyryloxy)-furoepaltol (**6**). White amorphous powder; TLC (petroleum ether/Me<sub>2</sub>CO, 3:1 v/v):  $R_f$  = 0.25; <sup>1</sup>H NMR (Me<sub>2</sub>CO, 500 MHz) see Table S2, <sup>13</sup>C NMR (Me<sub>2</sub>CO, 125 MHz) see Table S3, IR (KBr)  $\nu_{\max}$  3441, 2938, 1773, 1247, 1270 cm<sup>-1</sup>; HRESIMS ( $m/z$ ) [M+H]<sup>+</sup> calcd for C<sub>20</sub>H<sub>31</sub>O<sub>6</sub>, 367.2120; found 367.2122.

Crystal data for compound **3**. C<sub>20</sub>H<sub>28</sub>O<sub>5</sub>; MW = 348.42; monoclinic, space group *P*2<sub>1</sub>;  $a$  = 7.3794 (10) Å,  $b$  = 12.1840 (16) Å,  $c$  = 21.074 (3) Å,  $\alpha$  = 90.00,  $\beta$  = 90.00(10),  $\gamma$  = 90.00,  $V$  = 1894.8 (4) Å<sup>3</sup>,  $Z$  = 4,  $d$  = 1.221 g/cm<sup>3</sup>, crystal dimensions 0.27 × 0.19 × 0.14 mm was used for measurement on a SHELXL-97 with a graphite monochromator, Mo KR radiation. The total number of reflections measured was 4465, of which 2338 were observed,  $I > 2\sigma(I)$ . Final indices:  $R_1$  = 0.0510,  $wR_2$  = 0.1244. The crystal structure of **3** was resolved by the direct method SHLXS-97 (Sheldrick, 1990) and expanded using a difference Fourier technique, refined by the program SHLXL-97 (Sheldrick, 1997) and the full-matrix leastsquares calculations. Crystallographic data for the structure of **3** has been deposited in the Cambridge Crystallographic Data Centre (deposition number: CCDC 802641). Copies of the data can be obtained free of charge via [www.ccdc.cam.ac.uk/conts/retrieving.html](http://www.ccdc.cam.ac.uk/conts/retrieving.html) (or from the Cambridge Crystallographic Data Centre, 12, Union Road, Cambridge CB21EZ, U.K.; fax: (+44) 1223-336-033; or [deposit@ccdc.cam.ac.uk](mailto:deposit@ccdc.cam.ac.uk)).

#### S2.4. Quantitative HPLC-PDA analysis

The leaves were extracted in a refrigerator for 2 hours, and the samples concentrations were prepared to 10 or 50 mg (fresh leaf) /150  $\mu$ L, while compounds **1–6** were prepared to 0.1 mg/mL for HPLC-PDA quantification. HPLC-PDA analysis was performed using a gradient solvent system of H<sub>2</sub>O (A) and acetonitrile (B) as follows: 60–45% A over 20 min; kept 45% A from 20–45 min at a flow rate of 1 mL/min. Peaks were monitored by a PDA scanning device from 200 to 600 nm. The peak area for each compound was quantified and the standard was integrated from the HPLC-PDA chromatogram at 220 nm, and the concentration was calculated by using Waters Empower software (Figure S2).

### S3. Biological Activity Assay of Induced Furoeudesmanes

#### S3.1. Anti-inflammatory evaluation: xylene-induced ear edema in mice <sup>S3</sup>

Each mouse was given aspirin, pterodonic acid or placebo for 30 min before the induction of ear edema by topical application of 50  $\mu$ L xylene on both surfaces of the right ear. The left ear served as a control. Mice were sacrificed by cervical dislocation 1 h after xylene application. Ear disks of 8.0 mm in diameter were punched out and weighed (Table S1). The extent of edema was evaluated by the weight difference between the right and the left ear disks of the same animal. All animal procedures were approved by the Institutional Animal Care and Use Committee of Kunming Institute of Zoology, Chinese Academy of Sciences.

### S3.2. Insecticidal Assay

#### Insect Rearing

The larvae of the *Neurois renalba* were collected from *L. pterodonta* in the greenhouse, and reared in an environmental chamber held at 25°C under a photoperiod of 16 h/day. The second-instar larvae were selected for testing. The second-instar larvae of *Argyrogramma agnate*, *Spodoptera exigua*, *Pieris rapae* and third-instar larvae of *Plutella xylostella*, were collected from suburban vegetable fields of Kunming, Yunnan Province, China, and reared with cabbage (*Brassica oleracea* L.) in an environmental chamber at 25°C with 16 h/d photoperiod. Larvae of the second generation were reared to the second or third-instar for testing.

#### Antifeeding bioassay with leaf disk

Antifeeding activity was assayed according to the conventional leaf-disk methods.<sup>S4</sup> The test compounds were dissolved in acetone at a concentration of 1000  $\mu$ L/mL. Leaf disks ( $d = 6$  mm) of cabbage were dipped into the prepared solutions for 1s according to the method of Yee et al.<sup>S5</sup> Control disks were dipped into acetone. As a result, about 20  $\mu$ g test compounds adhered to each leaf disk and equal to 1.26  $\mu$ g/mg (fresh cabbage). The disks were allowed to stand on a plate to evaporate the acetone. One larva of *Argyrogramma agnate*, *Sodoptera exigua*, *Pieris rapae*, ten larvae of *Plutella xylostella* and eight disks were placed on a wet filter paper disk in a 9.0 cm diameter Petri dish. Three replicates were used for each compound. In the test, control and treated disks were placed in separate Petri dishes lined with moistened filter paper. After 24 h, the larvae were removed and disks were examined visually. The percentage of the area of the leaf disks consumed versus control was recorded. The antifeeding percentage was calculated as

antifeedancy =  $(CK - T)/CK \times 100\%$ . CK and *T* are control disk areas that were eaten and treated disk areas that were eaten, respectively.

The results of other testing showed that the larvae of *N. renalba* preferred leaves of *L. pterodonta* without the induced compounds in the greenhouse and in the disks testing (Figure S3).

### Serine protease inhibition assays

Serine protease inhibition assay was performed as described by Lai et al.<sup>S6</sup> The inhibitory effects of the tested compounds (30 nM) on the hydrolysis of synthetic chromogenic substrates by serine proteases were assayed in 50 mM Tris-HCl, pH 7.8 at room temperature. A trypsin-like serine protease was purified from mid-guts of the *Pieris rapae* and *Drosophila melanogaster*, respectively. The serine protease (final concentrations 10 nM) and different amounts of the tested compounds (final concentrations ranging from 0.01 to 10  $\mu$ M) were preincubated for 10 min at room temperature. T6140 (N-(p-Tosyl)-Gly-Pro-Lys-4-nitroanilide acetate salt, Sigma) and B-3133 (N-Benzoyl-Arg-4-nitroanilide-hydrochloride-pNA, Sigma) were used as a substrate, respectively. The reaction was initiated by the addition of the substrate to a final concentration of 0.5 mM. The formation of *p*-nitroaniline was monitored continuously at 405 nm for 5 min. The inhibition constant  $K_i$  of tested compounds for the hydrolysis of the substrate was determined according to the method of Dixon.<sup>S7</sup> Briefly, the inhibition assay was carried out as described above, and the  $K_i$  value was obtained by reciprocal plotting of the reaction velocity vs. inhibitor concentration under different substrate concentrations (0-2 mM).

### S3.3 Anti-tobacco mosaic virus (TMV) assays

#### Preparation of screening materials

*Nicotiana glutinosa* and *N. tabacum* cv.K<sub>326</sub> plants were cultivated in an insect-free greenhouse. *N. glutinosa* was used as a local lesion host, while *N. tabacum* cv.K<sub>326</sub> was used to determine systemic TMV infection. Plants with similar leaf-size and leaf-number were used for each experiment.

TMV (U1 strain) was propagated and maintained in the systemic *Nicotiana tabacum*

cv.K<sub>326</sub> and purified as described by Gooding and Hebert.<sup>S8</sup> The concentration of TMV was determined as 16 mg/mL with an ultraviolet spectrophotometer [virus concentration =  $(A_{260} \times \text{dilution ratio})/E_{1\text{cm}}^{0.1\%, 260\text{nm}}$ ]. The purified virus was kept at -20°C and was diluted to 32 µg/mL with 0.01 M phosphate sodium buffer before use.

The tested compounds were dissolved in DMSO and diluted with distilled H<sub>2</sub>O to the 100 µg/mL. The final concentration of DMSO was 25 µL/mL, and this did not adversely affect the plants. Ningnanmycin was used as a positive control, and 25 µL/mL DMSO solution was used as negative control. Healthy leaves or disks were immersed into 25 µL/mL DMSO solution as a further control procedure.

Half-leaf method <sup>S9</sup>

Growing leaves of *N. glutinosa* were mechanically inoculated with purified TMV (32 µg/mL). After 2 h, each leaf was cut along the main vein. One half of the leaf was immersed into a solution of the compound, and the other was immersed into 25 µL/mL DMSO solution as the negative control. Leaves were kept in a culture chamber at 25°C for 48 h, and then the rate of TMV inhibition was calculated as follows: Inhibition Rate (%) =  $[(C-T)/C] \times 100\%$ , where *C* and *T* are the average number of local lesions of the control and treatment, respectively. Three replicates were tested for each sample.

Leaf disk method <sup>S10</sup>

Growing leaves of *N. tabacum* cv.K<sub>326</sub> were mechanically inoculated with equal volumes of TMV (32 µg/mL). After 6 h, 1.2 cm diameter leaf discs were removed, and were floated on solutions of compounds, while the negative control was floated on 25 µL/mL DMSO solution. All leaf disks were kept in a culture chamber at 25°C for 48 h, and then the TMV concentration in the leaf disk was determined by TAS-ELISA. The inhibition rate of TMV was calculated as follows:  $(1 - \text{TMV concentration of treatment} / \text{TMV concentration of negative control}) \times 100\%$ . Three replicates were tested for each sample.

Triple Antibody Sandwich ELISA (TAS-ELISA)

TAS-ELISA was performed as described by Wang et al.<sup>S11</sup> A mouse monoclonal antibody

and a rabbit polyclonal antibody against TMV were prepared to construct the TAS-ELISA. In each 96-well plate, the wells were coated with 100  $\mu\text{L}$  polyclonal antibody in coating buffer (15  $\mu\text{mol/L}$   $\text{Na}_2\text{CO}_3$ , 35  $\mu\text{mol/L}$   $\text{NaHCO}_3$ , pH 9.6) for 3 h at 37°C, then the solution was removed and the wells were washed three times with phosphate buffer containing 0.5% Tween 20 (PBST). The antigen solution consisted of leaf disks ground in PBST. The antigen solution was added to the wells (100  $\mu\text{L}$  per well) and incubated for 3 h at 37°C, then the solution was removed and wells were washed four times with PBST. Blocking solution (200  $\mu\text{L}$  of 2% albumin bovine V in PBST) was added to each well and the plate was incubated for 40 min at 37°C. The wells were then washed three times with PBST before addition of 100  $\mu\text{L}$  mixed solution of monoclonal antibody and peroxidase-conjugated secondary antibody (goat antimouse IgG) (Sigma, St. Louis, MO) in PBST. Plates were then incubated for 3 h at 37°C, before washing a further three times with PBST. Plates were developed by adding 100  $\mu\text{L}$  of 1mg/mL 4-nitrophenyl phosphate bis-(cyclohexylammonium) salt in 10% diethanolamine. The absorbance value was measured at 405 nm using an ELISA plate reader (Bio-TEK, Winooski, VT).

#### SDS-PAGE and Western Blot Analysis of TMV Coat Protein (CP)

SDS-PAGE was performed as described by Sambrook et al.<sup>S12</sup> Briefly, leaf disks from the leaf-disk method were ground in protein loading buffer (40 g/L SDS, 10 ml/L  $\beta$ -ME, 200 ml/L glycerin, 2 g/L bromophenol blue, 0.1 mol/L Tris-HCl, pH 6.8) and then 5  $\mu\text{L}$  of samples and 3  $\mu\text{L}$  of marker were loaded on a polyacrylamide gel (5% stacking gel, 12.5% separating gel). Samples were run in duplicate. After SDS-PAGE, TMV protein bands were transferred at 150 mA for 75 min onto a nitrocellulose membrane (0.2  $\mu\text{M}$ ) using an electrotransfer system (Bio-Rad, Hercules, CA). The membrane was washed in TBST (1 mol/L Tris-HCl, pH 7.5; 1 mol/L NaCl; 0.05% Tween-20) and blocked with 2% albumin bovine V in TBST for 1 h at 37°C. The membrane was washed three times for 15 min with TBST and reacted with a mixture of 1:6000 polyclonal antibodies of TMV and 1:5000 alkaline phosphataseconjugated antirabbit IgG (Sigma, St. Louis, MO) for 1 h at 37°C. Next, it was washed three times for 15 min with TBST and the membrane incubated in substrate buffer (1 mol/L Tris-HCl, pH 9.5; 1mol/L NaCl; 1mol/L  $\text{MgCl}_2$ ) with 330  $\mu\text{L/mL}$  NBT and 165  $\mu\text{L/mL}$  BCIP for 3-5 min in the dark until the bands of CP were clear.

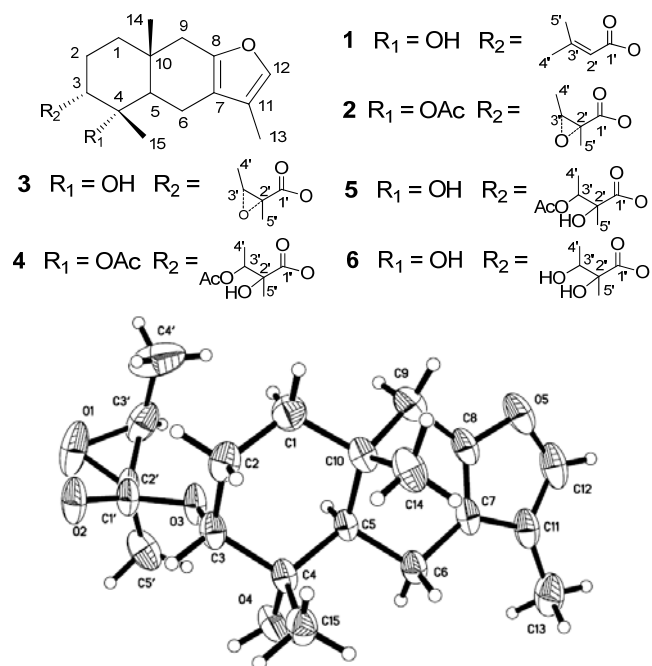


**Figure S1.** Structures of the six induced furoudesmanes (1–6), and the configuration of 3 by X-ray diffraction.

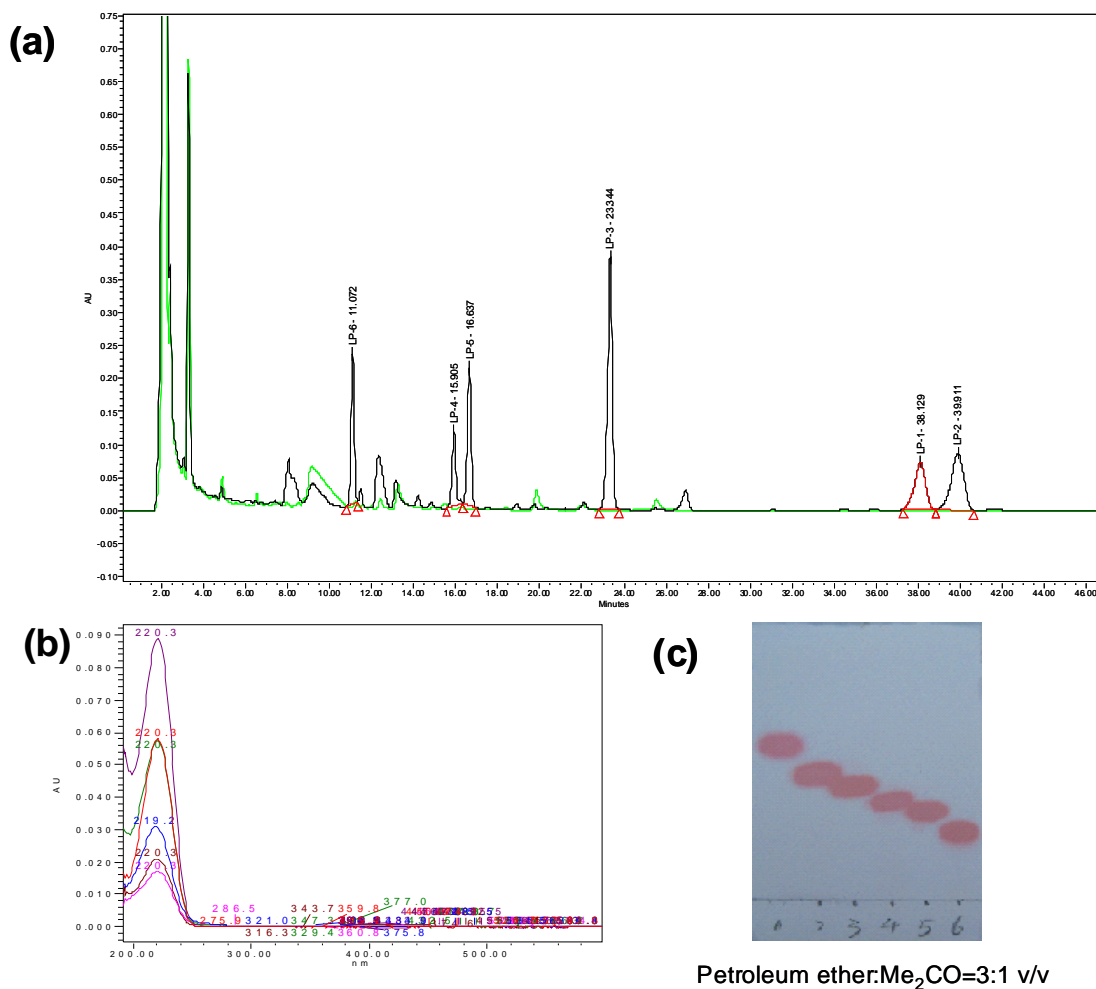


**Figure S2.** The concentrations of the six induced compounds in fresh induced leaves. (a) Overlapped HPLC profiles of acetone extract of *L. pterodonta* (black curve represents the treated group, while green represents the unwounded group; at a concentration of 10 mg fresh leaf/150  $\mu$ L). (b) Overlapped UV spectra of the six induced compounds extracted from PDA. (c) The TLC profiles of six induced furoeudesmanes 1–6 (petroleum ether/ $\text{Me}_2\text{CO}$ , 3:1 v/v).

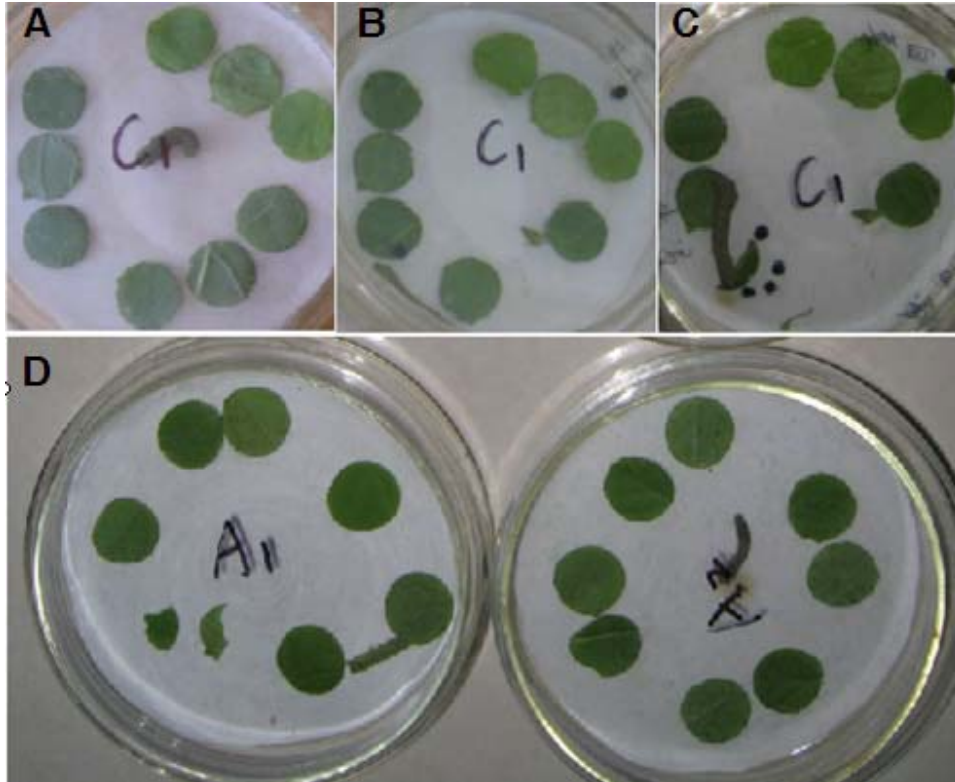


**Figure S3.** The larvae of *N. renalba* prefer leaves of *L. pterodonta* without induced compounds. **(A)** 0 h: *N. renalba* was placed in the middle of the dish containing nine leaves (leaves 1–3, *L. pterodonta* with the induced compounds; leaves 4–6, *L. pterodonta* without the induced compounds; leaves 7–9, cabbage [*Brassica oleracea* L.]). **(B)** 4 h later: *N. renalba* ate a piece of leaf of *L. pterodonta* without the induced compounds (leaf 5). **(C)** 8 h later: *N. renalba* ate another piece of leaf of *L. pterodonta* without the induced compounds (leaf 4) and half piece of leaf of *L. pterodonta* with the induced compounds (leaf 3). In all three independent experiments, the larvae of *N. renalba* did not attack any cabbage leaves. **(D)** Two reared second-instar larvae of *N. renalba* were fed with leaves of *L. pterodonta* without the induced compounds (A1; left dish) and with the induced compounds (A2; right dish). Four hours later, the leaves containing the induced compounds (A2) were still intact, while two leaves of *L. pterodonta* without the induced compounds had been almost fully consumed (A1).

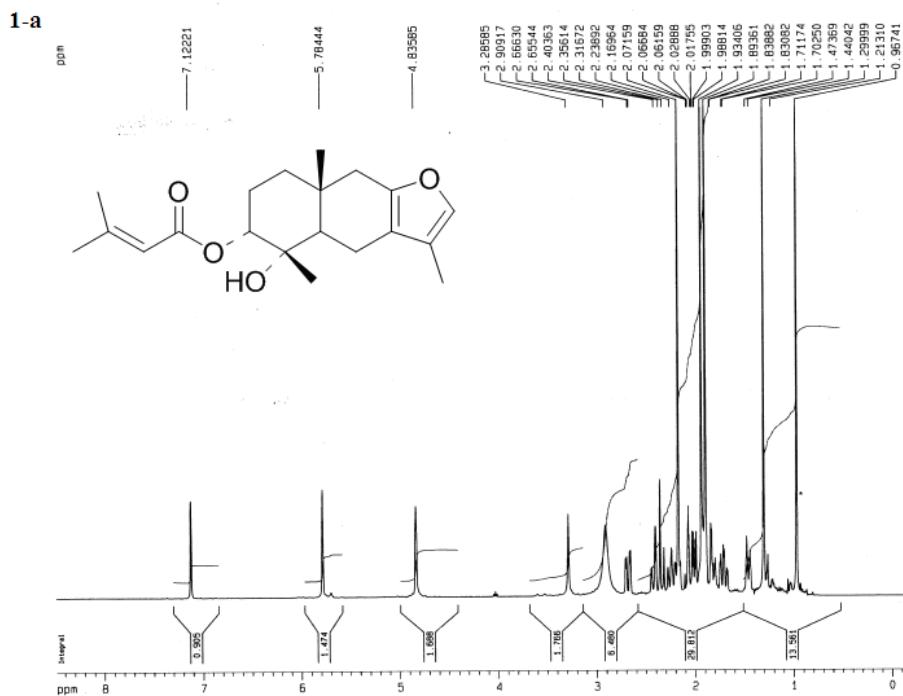


**Figure S4.** The  $^1\text{H}$  NMR of  $3\alpha$ -(2'(3')-ene-3'-methylbutyryloxy)-furoepaltol (**1**).

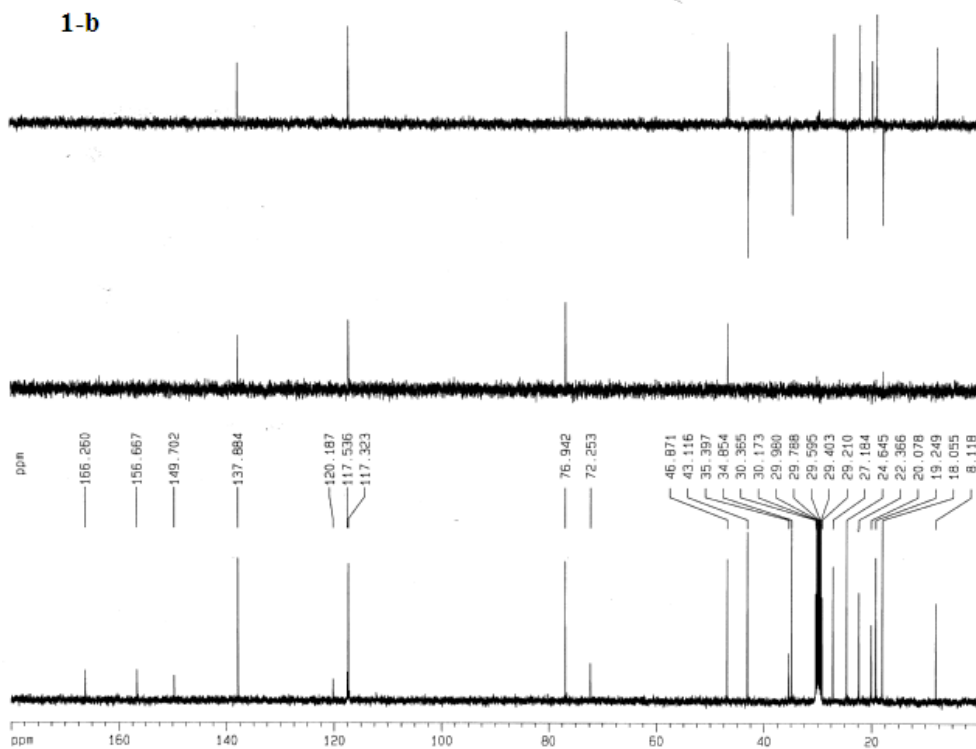


**Figure S5.** The  $^{13}\text{C}$  NMR of  $3\alpha$ -(2'(3')-ene-3'-methylbutyryloxy)-furoepaltol (**1**).

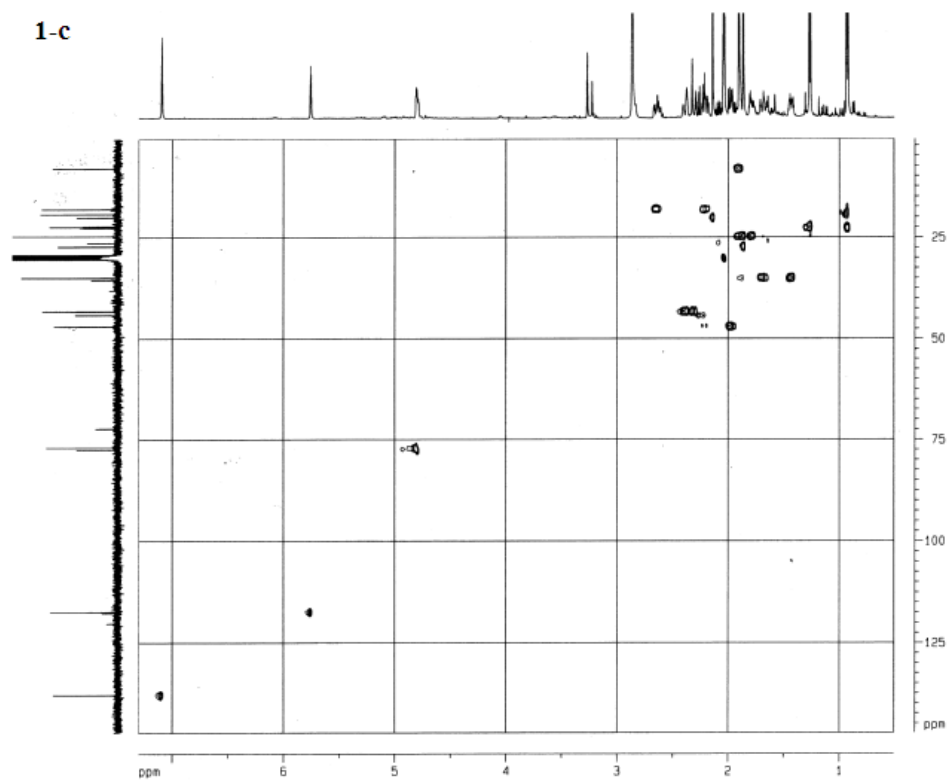


Figure S6. The HSQC of  $3\alpha$ -(2'(3')-ene-3'-methylbutyryloxy)-furoepaltol (**1**).

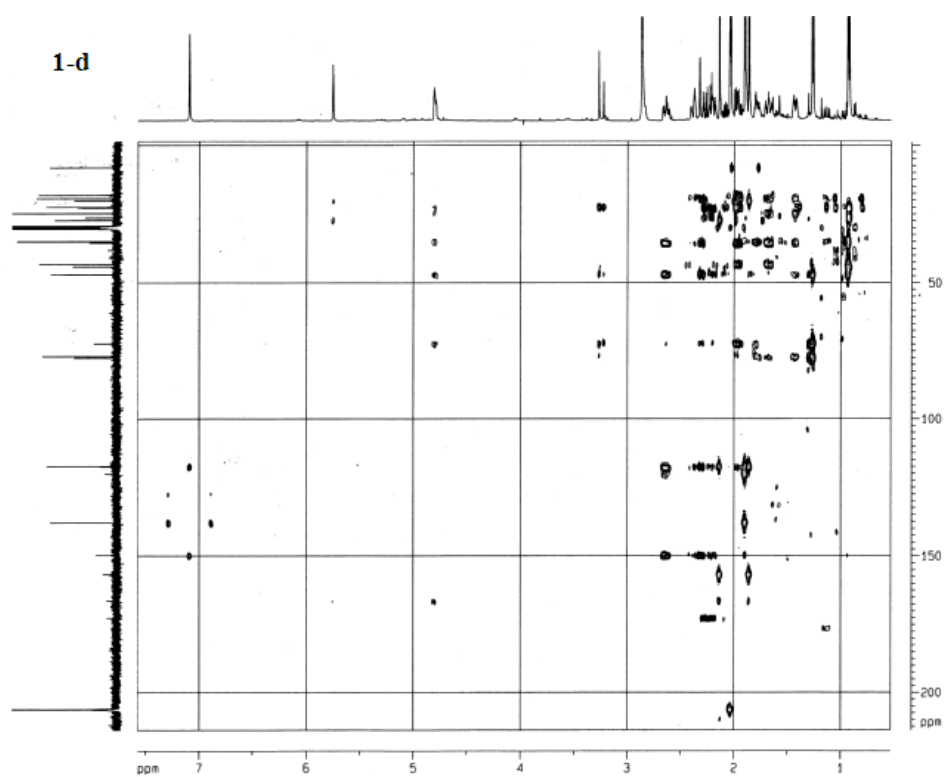
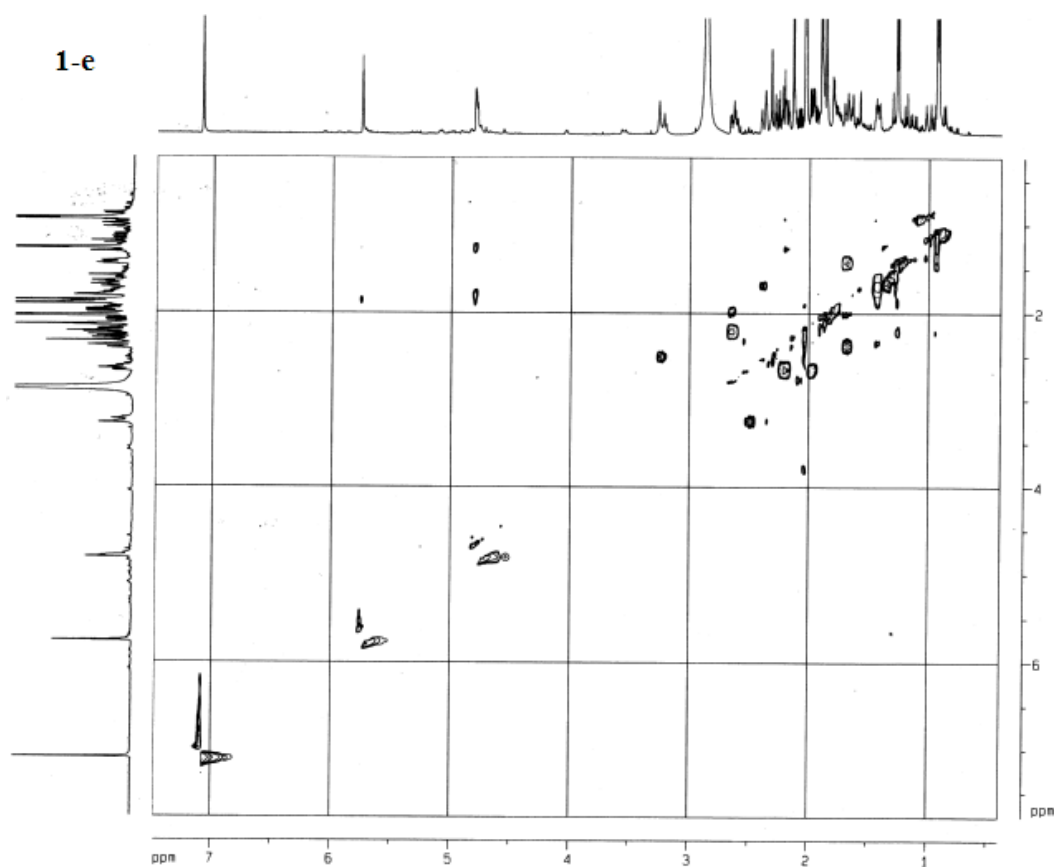
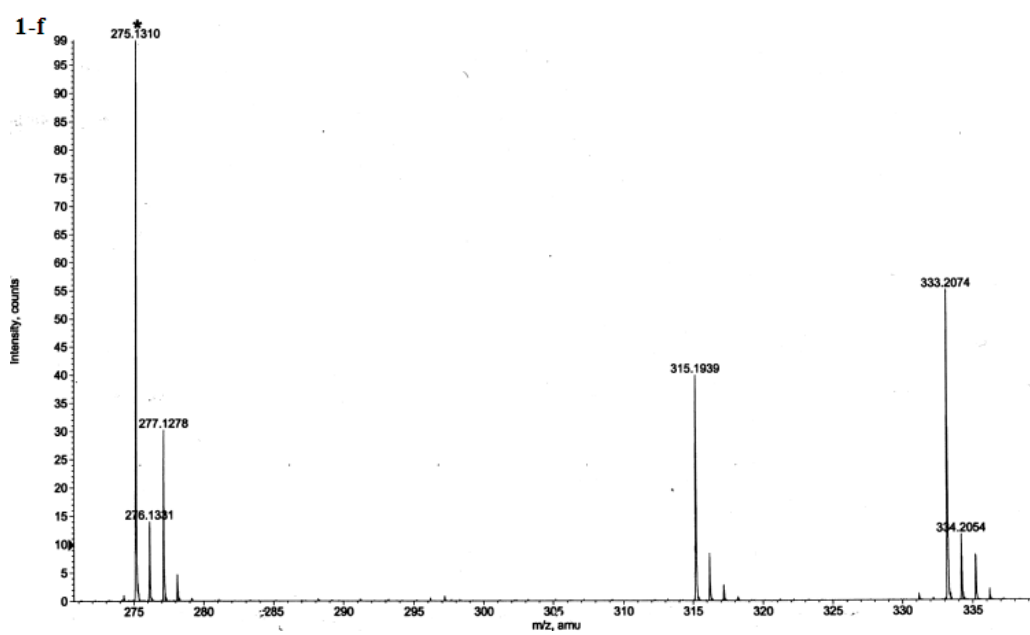


Figure S7. The HMBC of  $3\alpha$ -(2'(3')-ene-3'-methylbutyryloxy)-furoepaltol (**1**).



**Figure S8.** The ROESY of  $3\alpha$ -(2'(3')-ene-3'-methylbutyryloxy)-furoepaltol (**1**).



**Figure S9.** The HREIMS of  $3\alpha$ -(2'(3')-ene-3'-methylbutyryloxy)-furoepaltol (**1**).

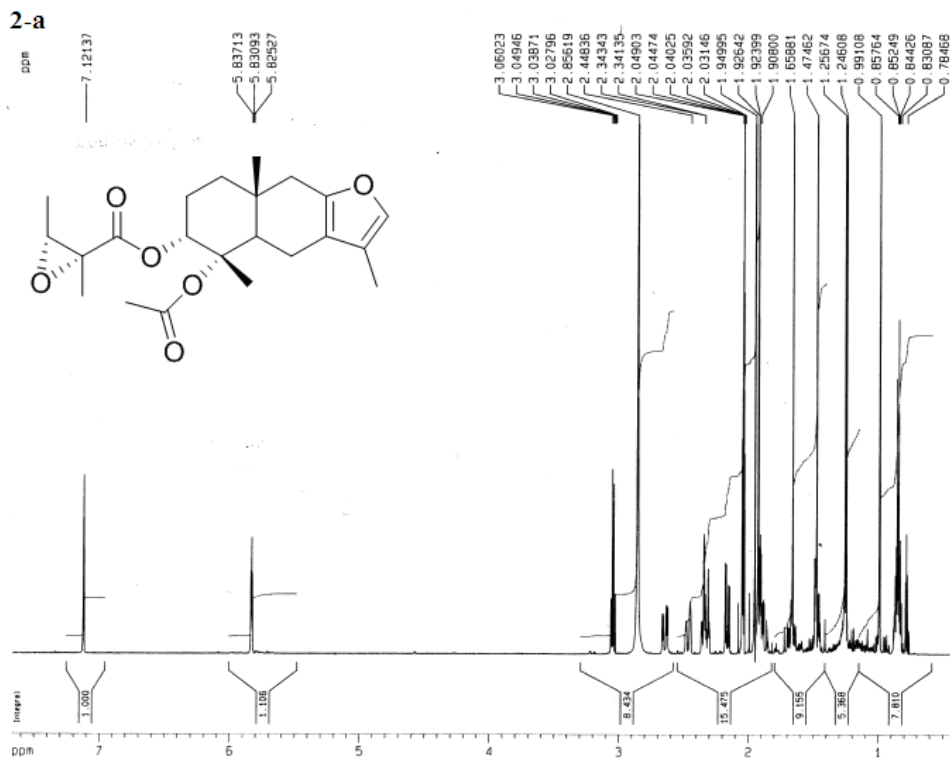


**Figure S10.** The  $^1\text{H}$  NMR of  $3\alpha$ -( $2\alpha'$ , $3\alpha'$ -epoxy-2'-methylbutyryloxy)- $4\alpha$ -acetyfuroepaltol (**2**).

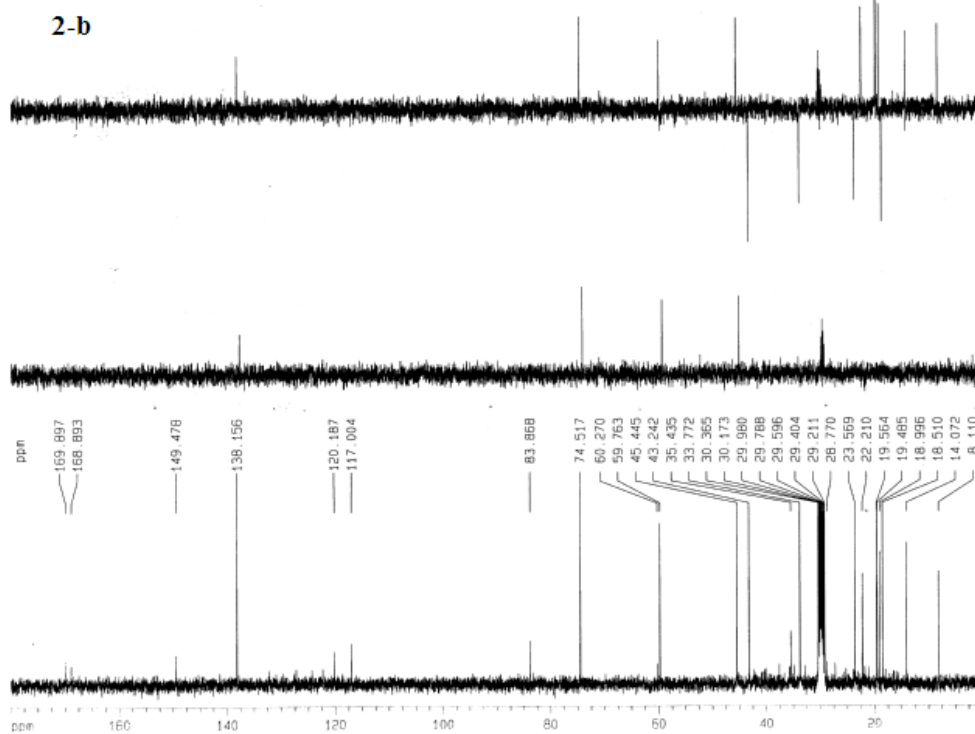


**Figure S11.** The  $^{13}\text{C}$  NMR of  $3\alpha$ -( $2\alpha'$ , $3\alpha'$ -epoxy-2'-methylbutyryloxy)- $4\alpha$ -acetyfuroepaltol (**2**).

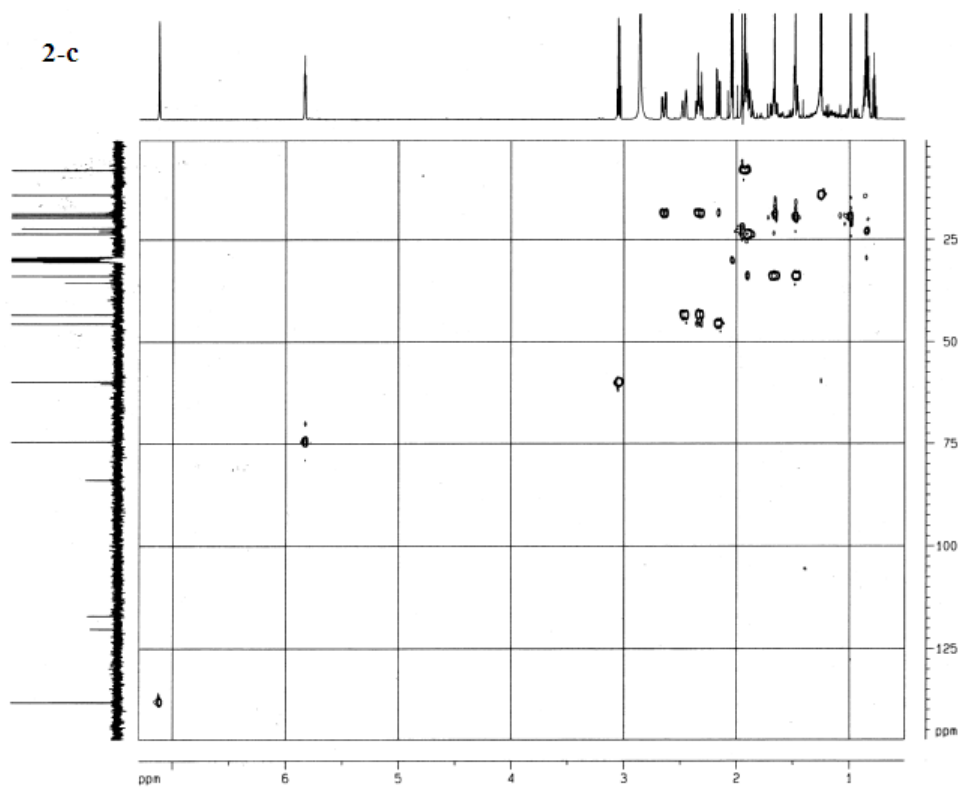


Figure S12. The HSQC of  $3\alpha$ -( $2\alpha'$ , $3\alpha'$ -epoxy-2'-methylbutyryloxy)- $4\alpha$ -acetyfuroepaltol (**2**).

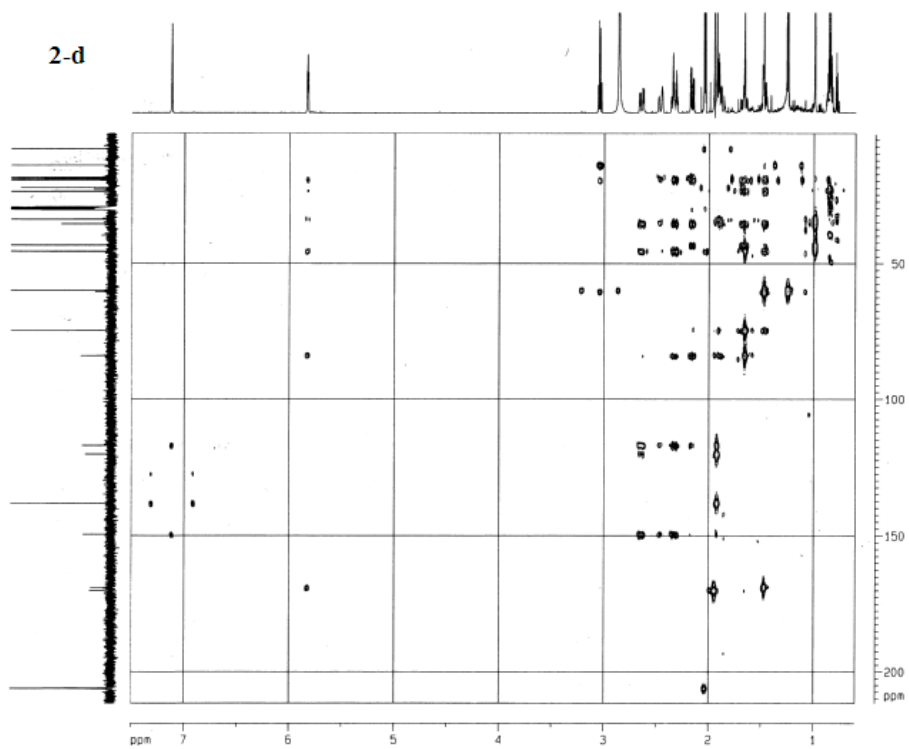
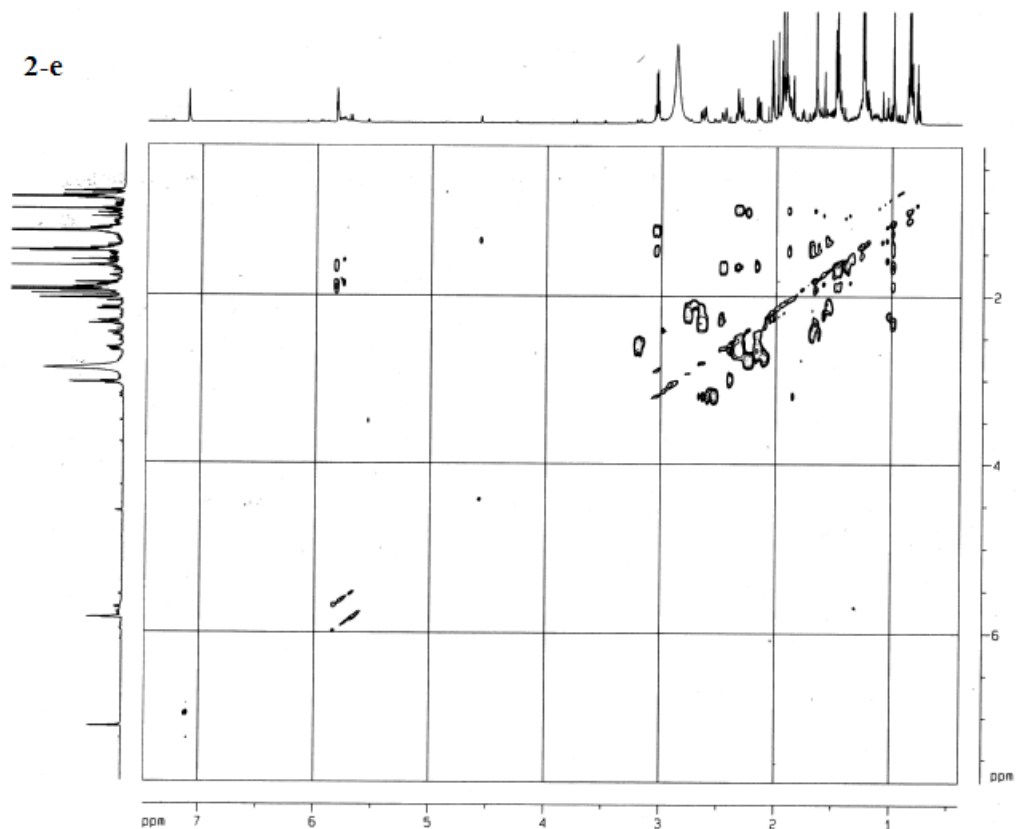
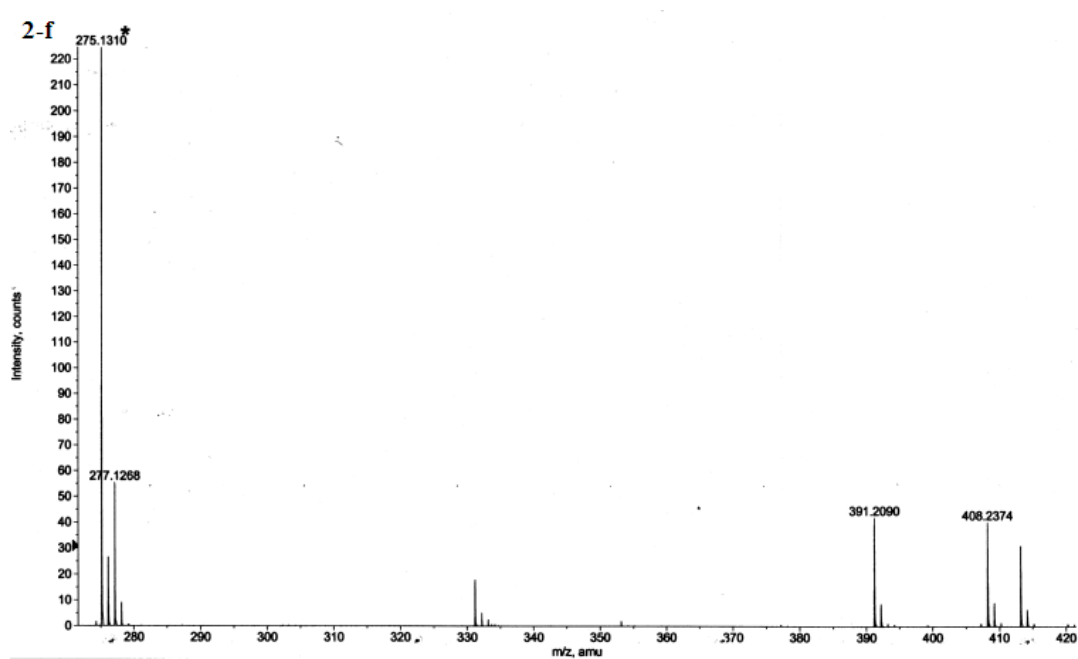


Figure S13. The HMBC of  $3\alpha$ -( $2\alpha'$ , $3\alpha'$ -epoxy-2'-methylbutyryloxy)- $4\alpha$ -acetyfuroepaltol (**2**).



**Figure S14.** The ROESY of  $3\alpha$ -( $2\alpha'$ , $3\alpha'$ -epoxy-2'-methylbutyryloxy)- $4\alpha$ -acetyfuroepaltol (**2**).



**Figure S15.** The HREIMS of  $3\alpha$ -( $2\alpha'$ , $3\alpha'$ -epoxy-2'-methylbutyryloxy)- $4\alpha$ -acetyfuroepaltol (**2**).

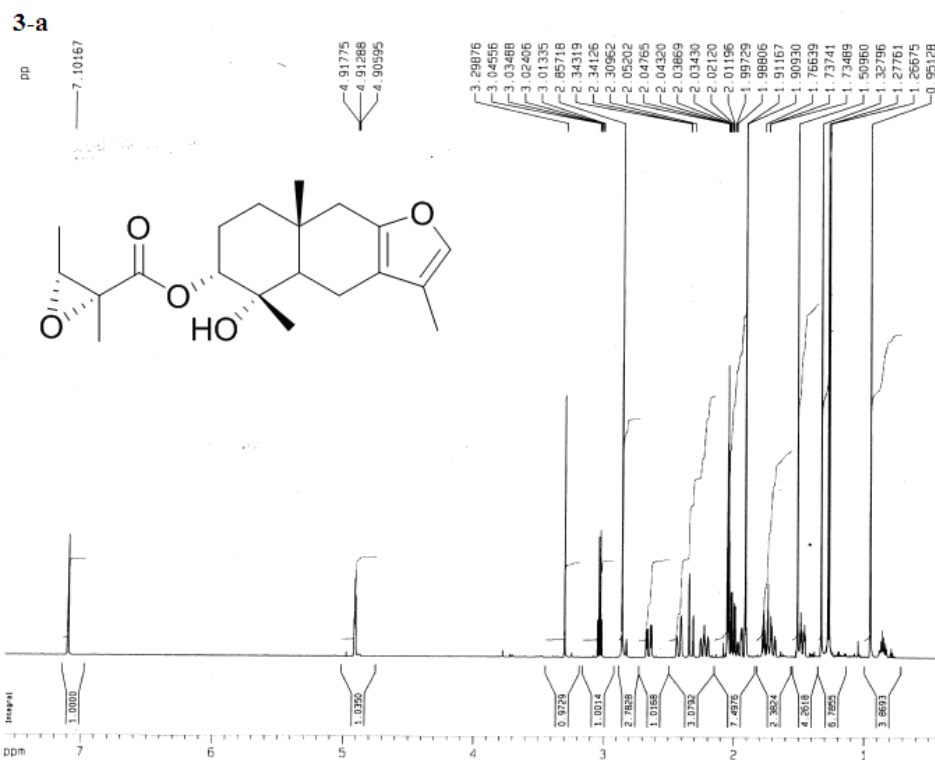


**Figure S16** The  $^1\text{H}$  NMR of  $3\alpha$ -(2 $\alpha$ ',3 $\alpha$ '-epoxy-2'-methylbutyryloxy)-furoepaltol (3).

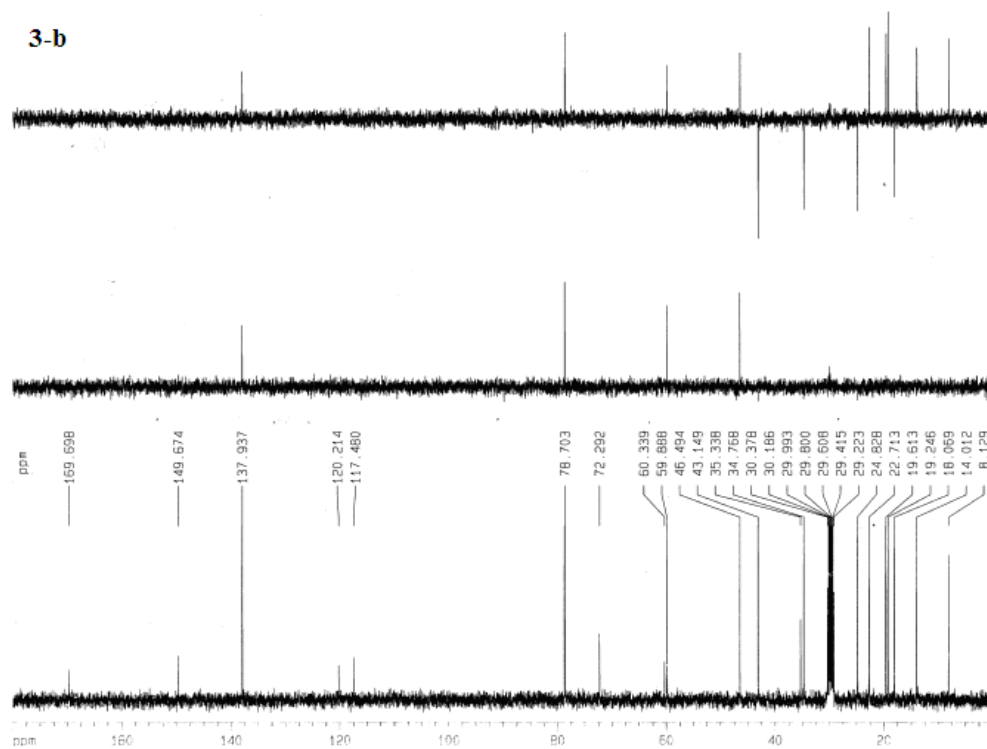


**Figure S17.** The  $^{13}\text{C}$  NMR of  $3\alpha$ -(2 $\alpha$ ',3 $\alpha$ '-epoxy-2'-methylbutyryloxy)-furoepaltol (3).

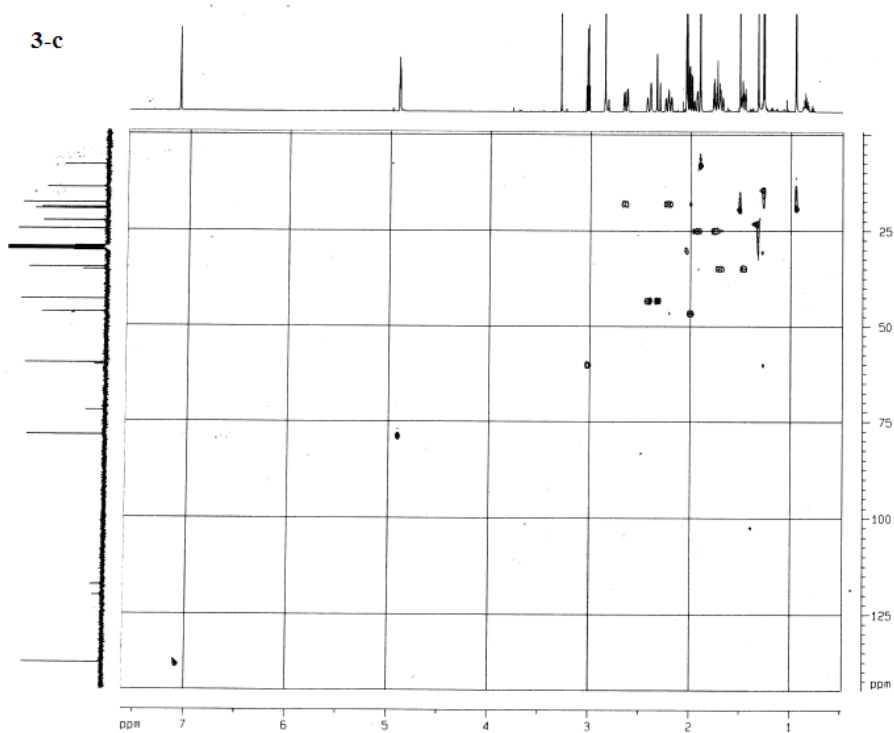


Figure S18 The HSQC of  $3\alpha$ -( $2\alpha'$ , $3\alpha'$ -epoxy-2'-methylbutyryloxy)-furoepaltol (**3**).

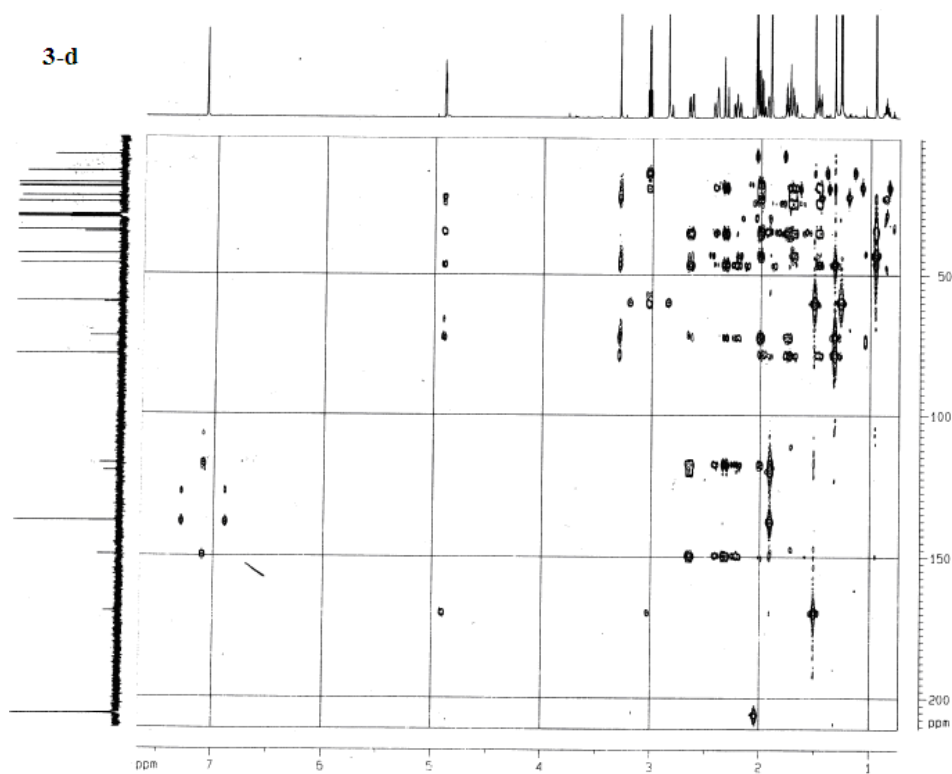
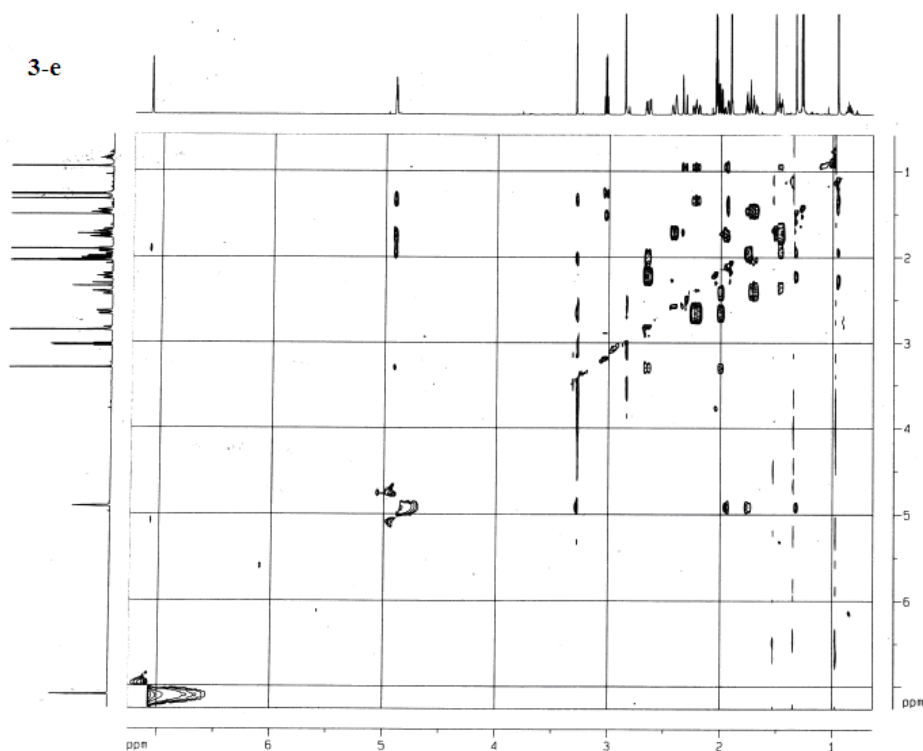
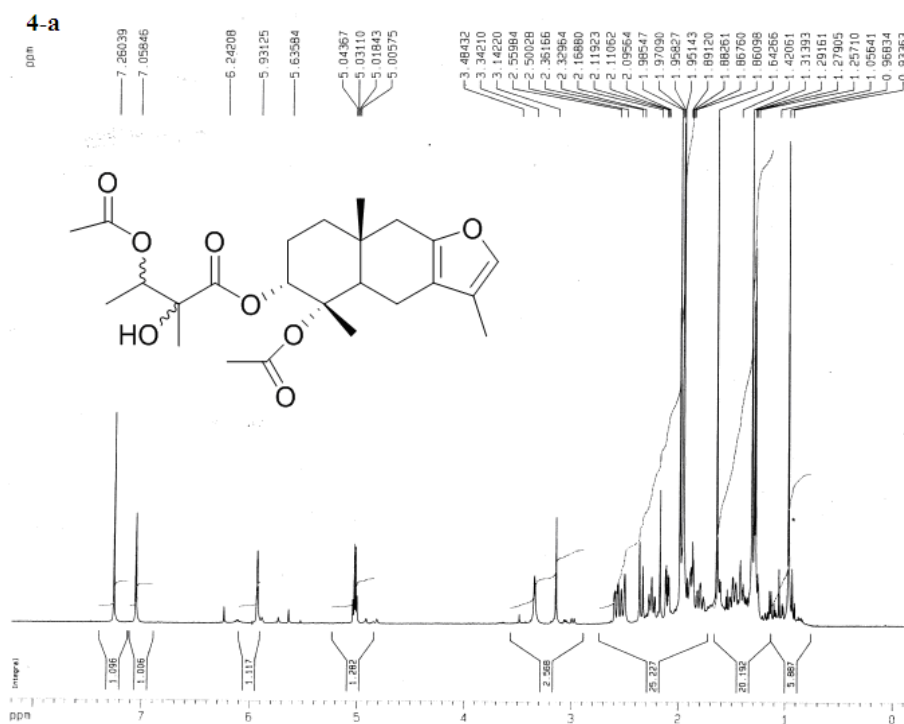


Figure S19. The HMBC of  $3\alpha$ -( $2\alpha'$ , $3\alpha'$ -epoxy-2'-methylbutyryloxy)-furoepaltol (**3**).



**Figure S20.** The ROESY of  $3\alpha$ -(2 $\alpha'$ ,3 $\alpha'$ -epoxy-2'-methylbutyryloxy)-furoepaltol (**3**).



**Figure S21.**  $^1\text{H}$  NMR of  $3\alpha$ -(2'-hydroxy-2'-methyl-3'-acetoxybutyryloxy)-4 $\alpha$ -acetyfuroepaltol (**4**).

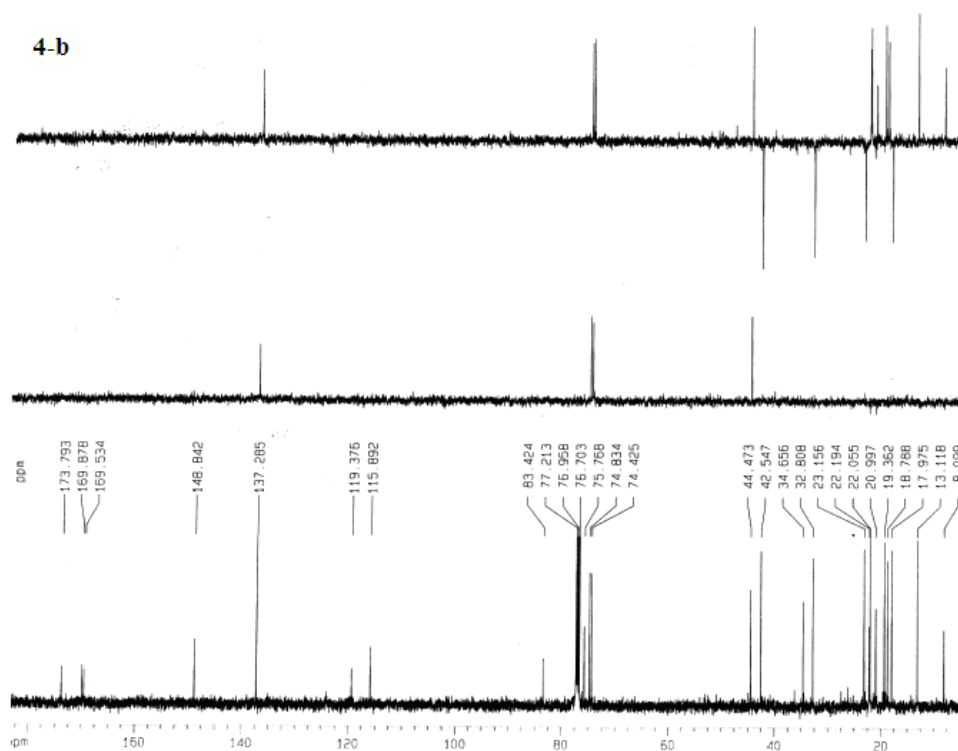


**Figure S22.**  $^{13}\text{C}$ NMR of  $3\alpha$ -(2'-hydroxy-2'-methyl-3'-acetoxybutyryloxy)- $4\alpha$ -acetyfuroepaltol (4).

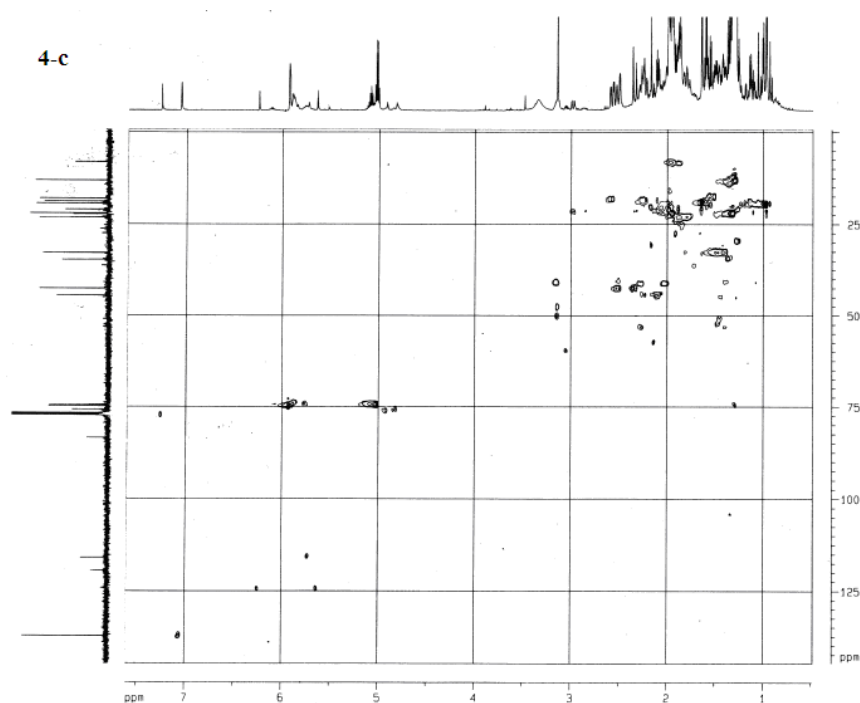


**Figure S23.** HSQC of  $3\alpha$ -(2'-hydroxy-2'-methyl-3'-acetoxybutyryloxy)- $4\alpha$ -acetyfuroepaltol (4).

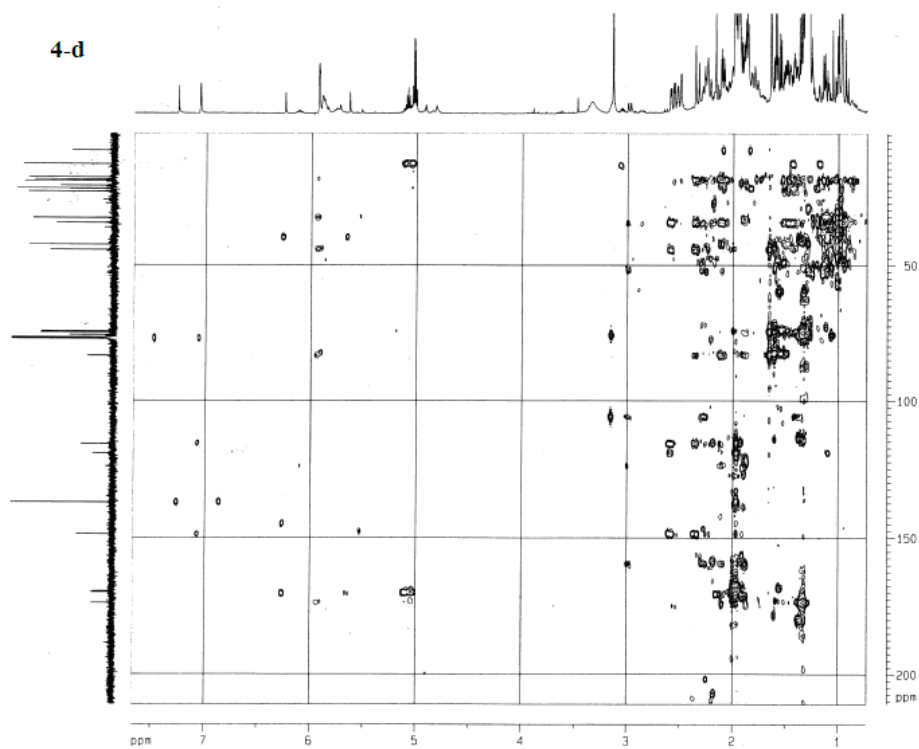


Figure S24. HMBC of  $3\alpha$ -(2'-hydroxy-2'-methyl-3'-acetoxybutyryloxy)- $4\alpha$ -acetyfuroepaltol (**4**).

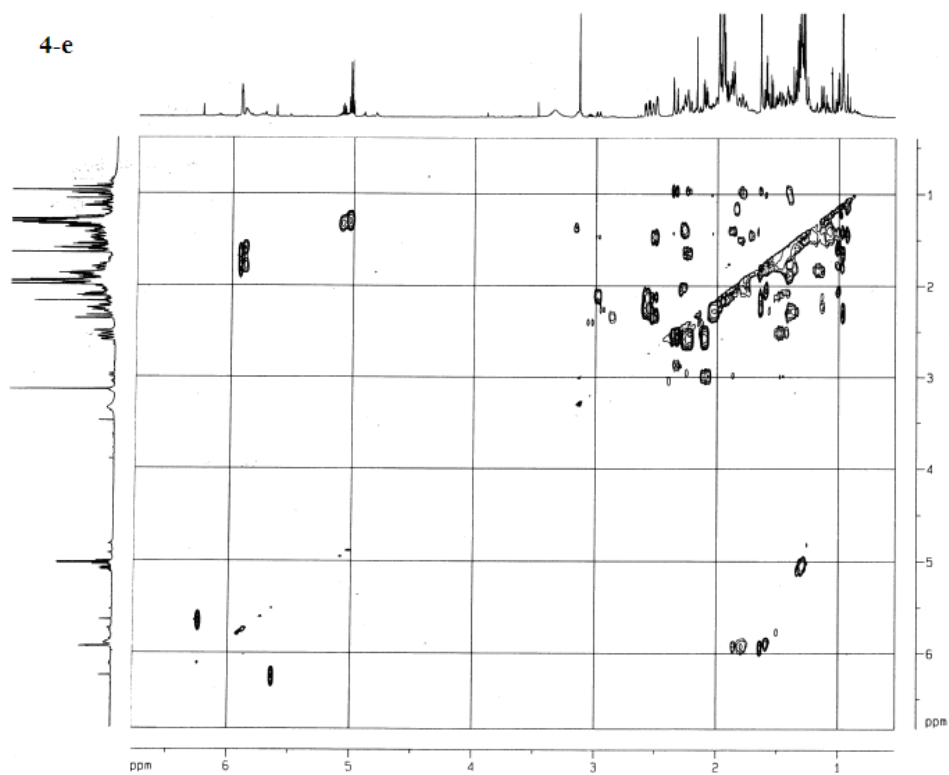
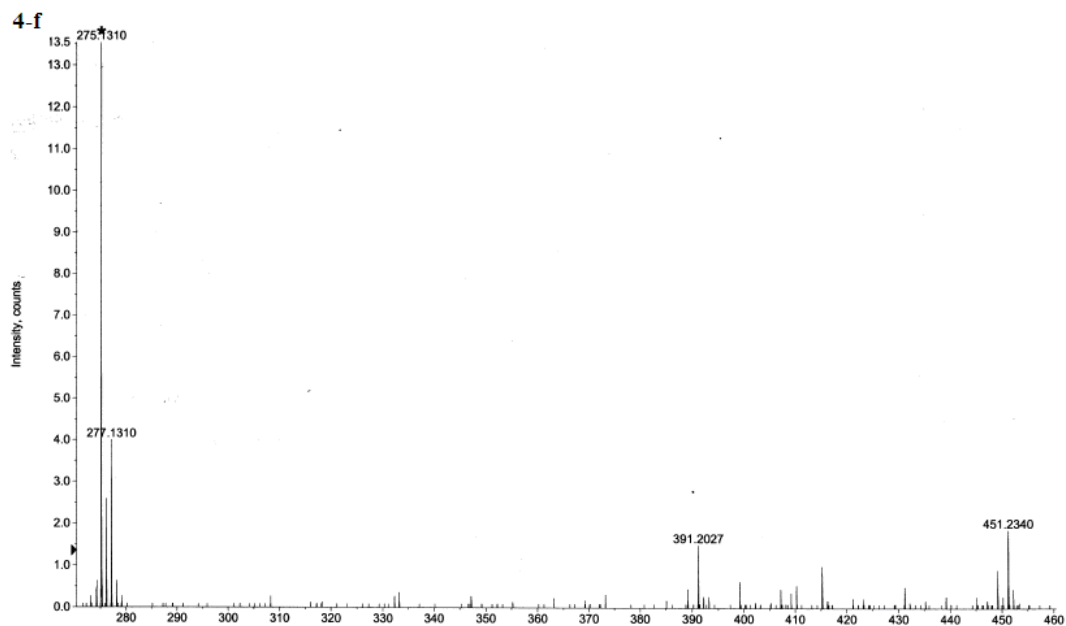
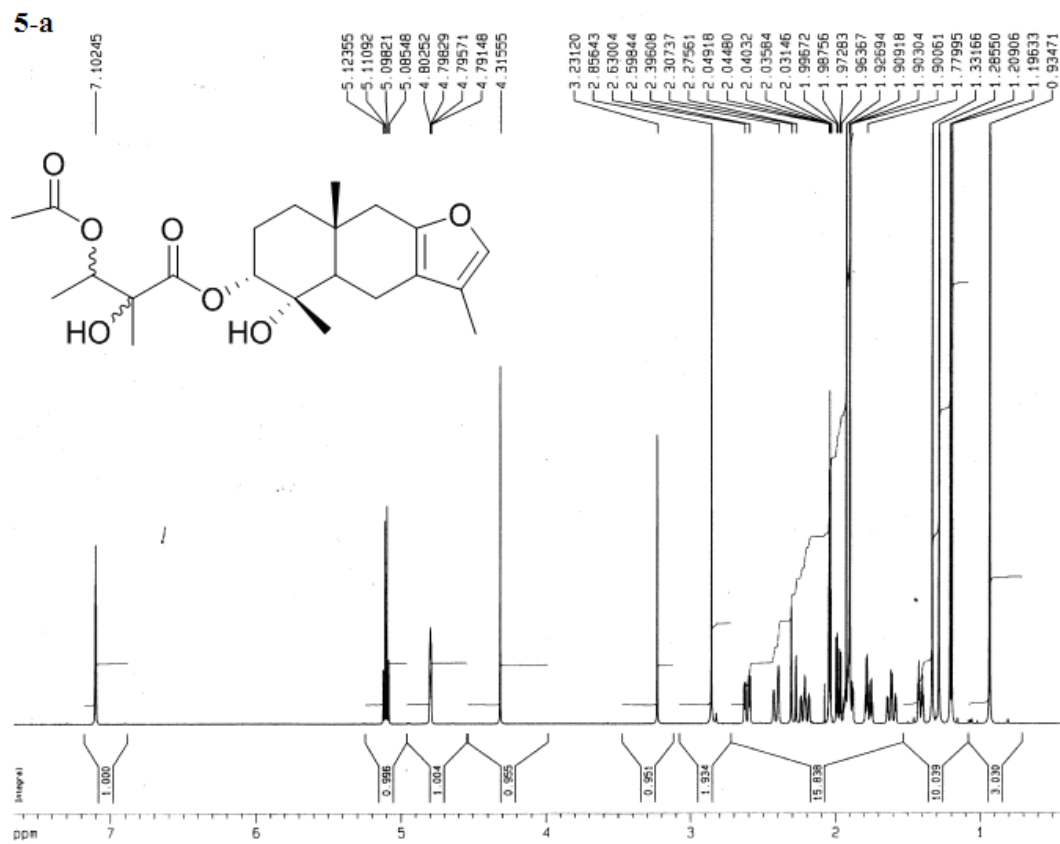


Figure S25. ROESY of  $3\alpha$ -(2'-hydroxy-2'-methyl-3'-acetoxybutyryloxy)- $4\alpha$ -acetyfuroepaltol (**4**).



**Figure S26.** HREIMS of  $3\alpha$ -(2'-hydroxy-2'-methyl-3'-acetoxybutyryloxy)- $4\alpha$ -acetyfuroepaltol (4).



**Figure S27.** The  $^1\text{H}$  NMR of  $3\alpha$ -(2'-hydroxy-2'-methyl-3'-acetoxybutyryloxy)-furoepaltol (5).

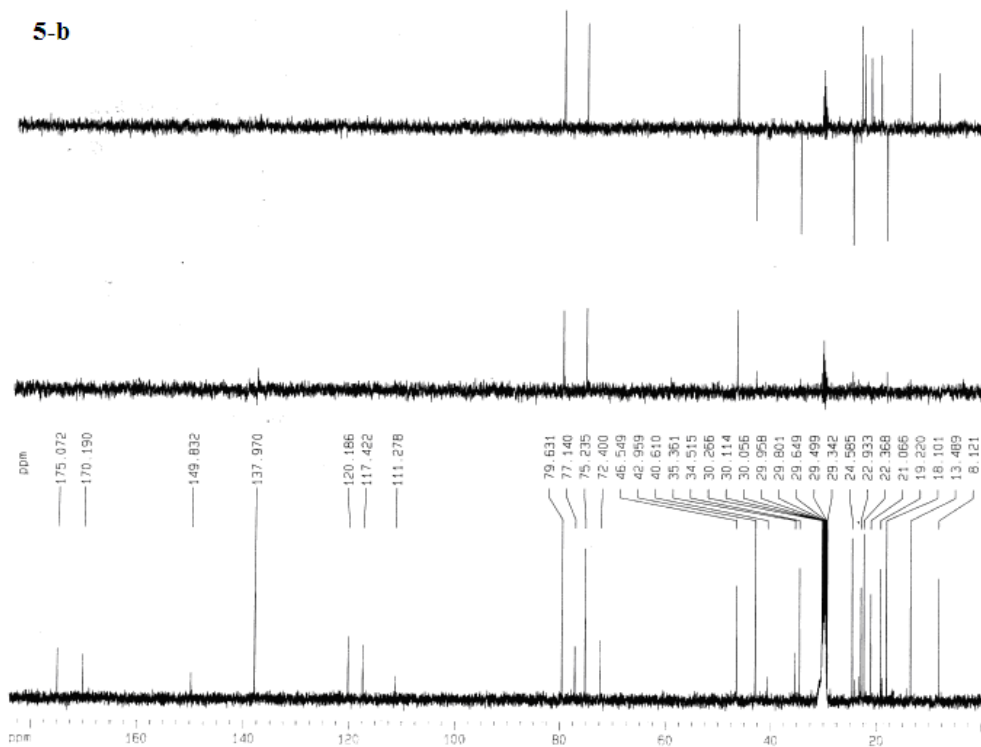


**Figure S28.** The  $^{13}\text{C}$  NMR of  $3\alpha$ -(2'-hydroxy-2'-methyl-3'-acetoxybutyryloxy)-furoepaltol (**5**).

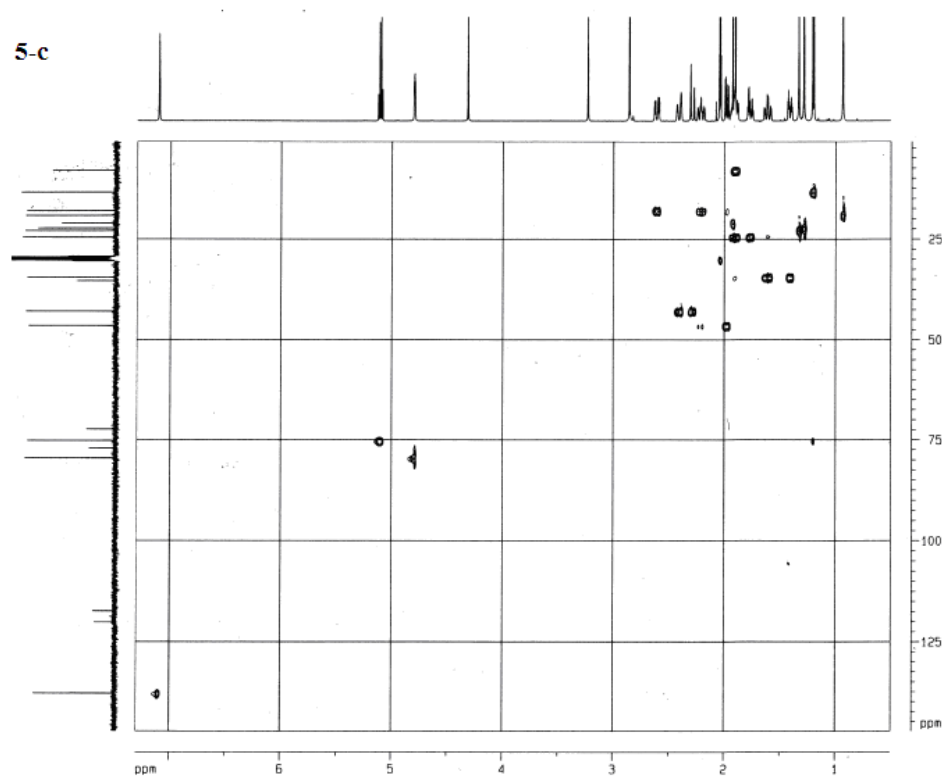


**Figure S29.** The HSQC of  $3\alpha$ -(2'-hydroxy-2'-methyl-3'-acetoxybutyryloxy)-furoepaltol (**5**).

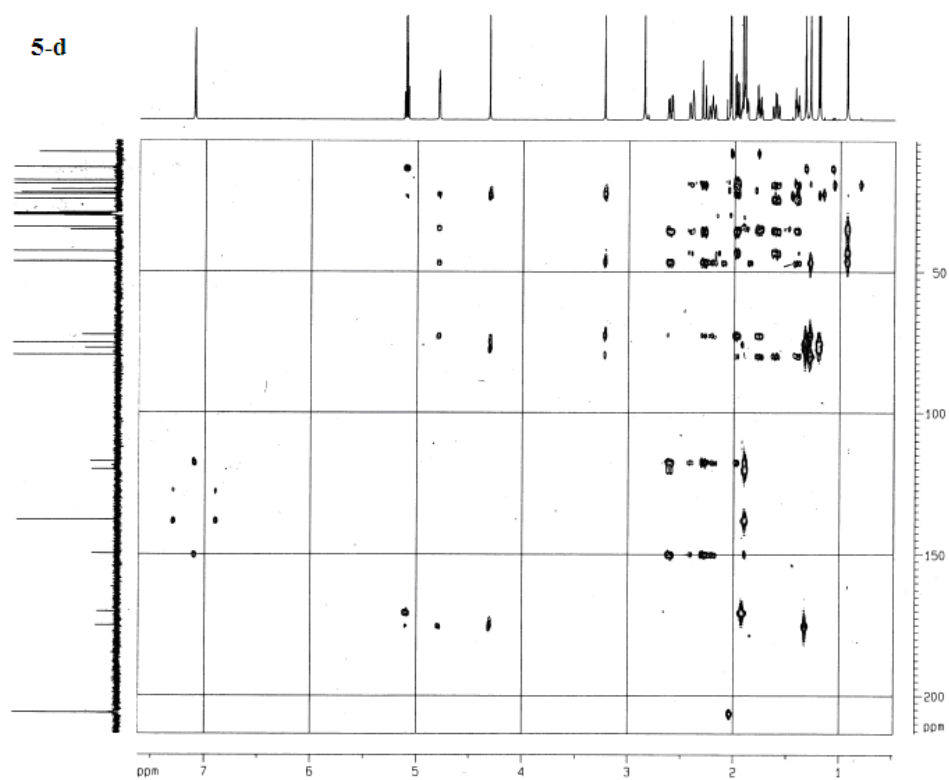


Figure S30. The HMBC of  $3\alpha$ -(2'-hydroxy-2'-methyl-3'-acetoxybutyryloxy)-furoepaltol (**5**).

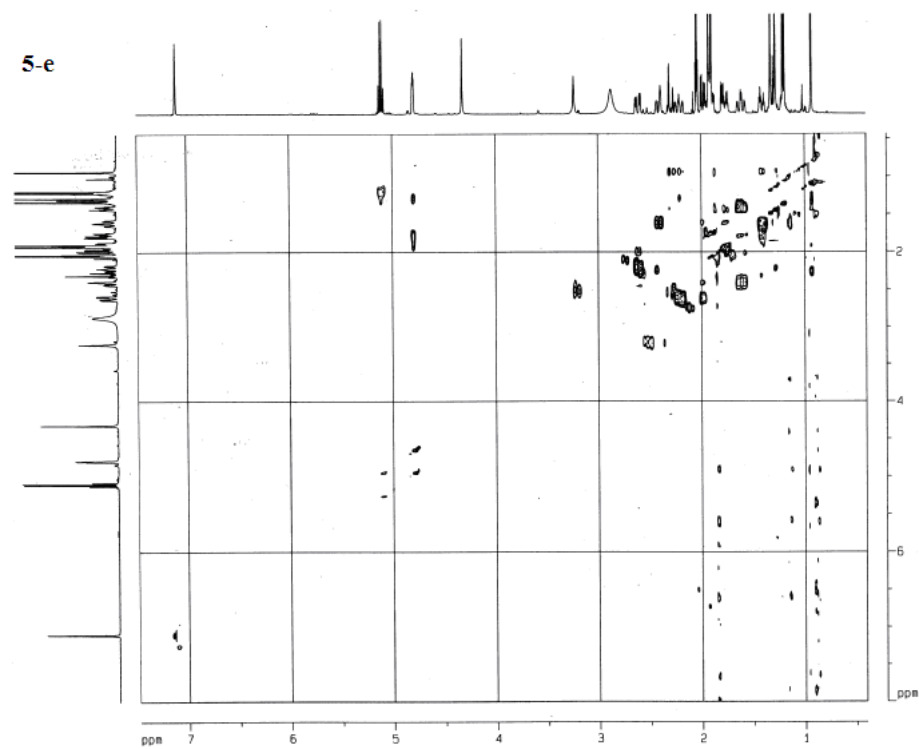
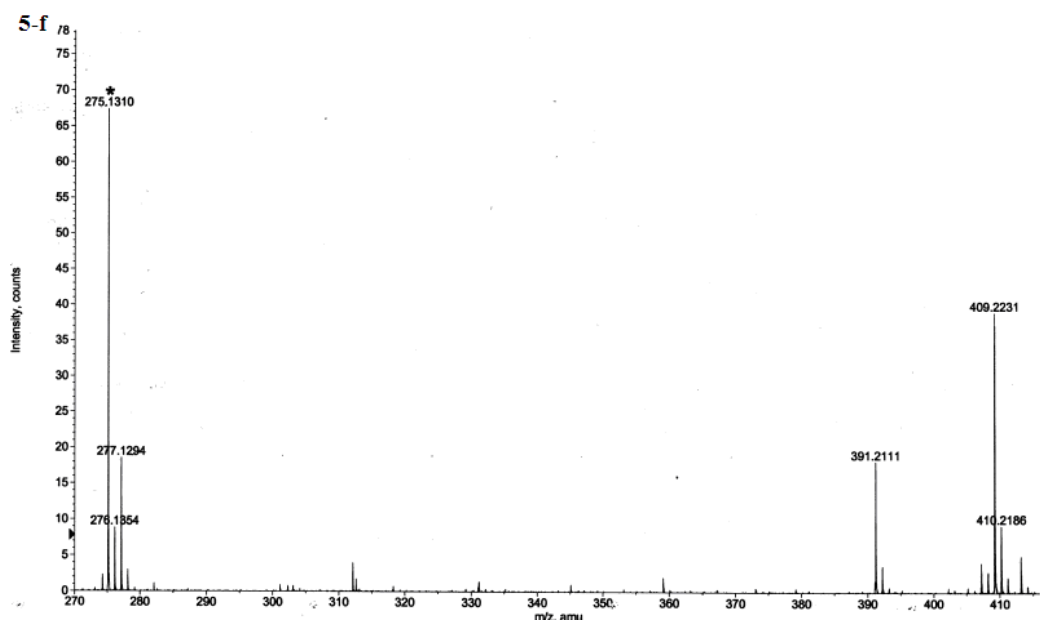
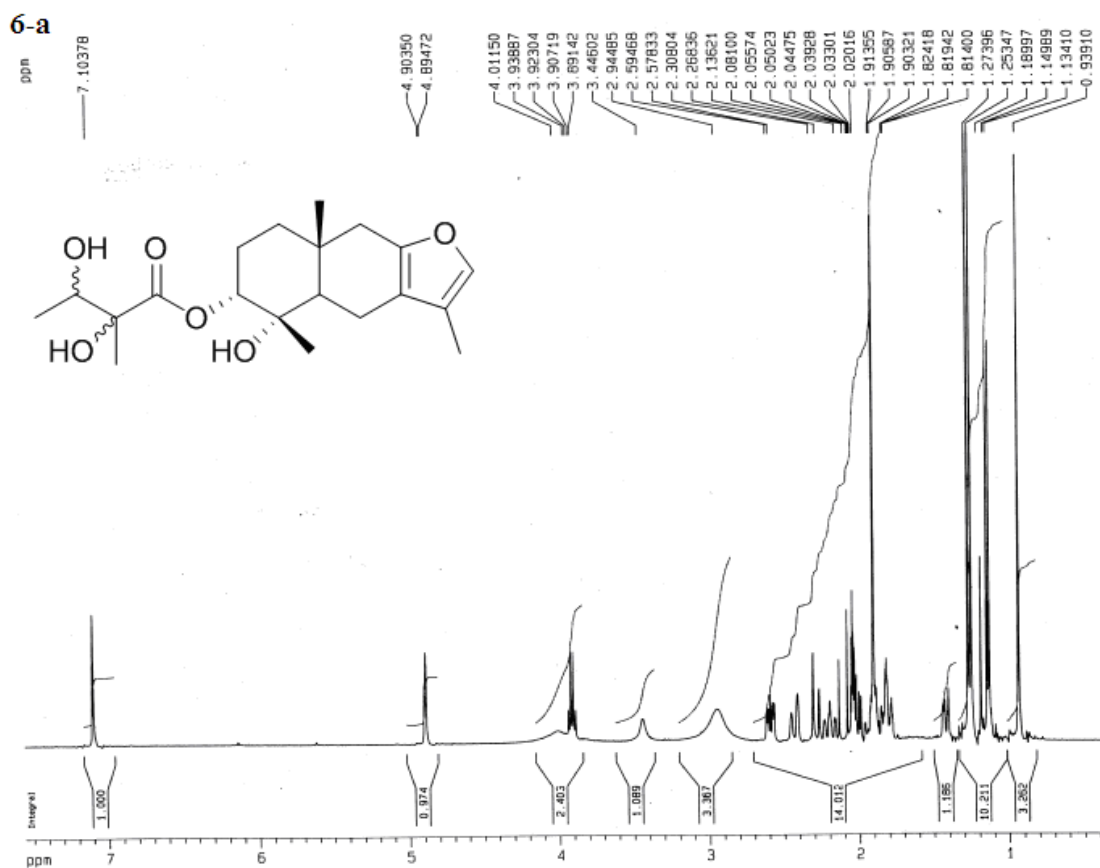


Figure S31. The ROESY of  $3\alpha$ -(2'-hydroxy-2'-methyl-3'-acetoxybutyryloxy)-furoepaltol (**5**).



**Figure S32.** The HREIMS of 3 $\alpha$ -(2'-hydroxy-2'-methyl-3'-acetoxybutyryloxy)-furoepaltol (**5**).



**Figure S33.** The  $^1\text{H}$  NMR of 3 $\alpha$ -(2',3'-dihydroxy-2'-methylbutyryloxy)-furoepaltol (**6**).

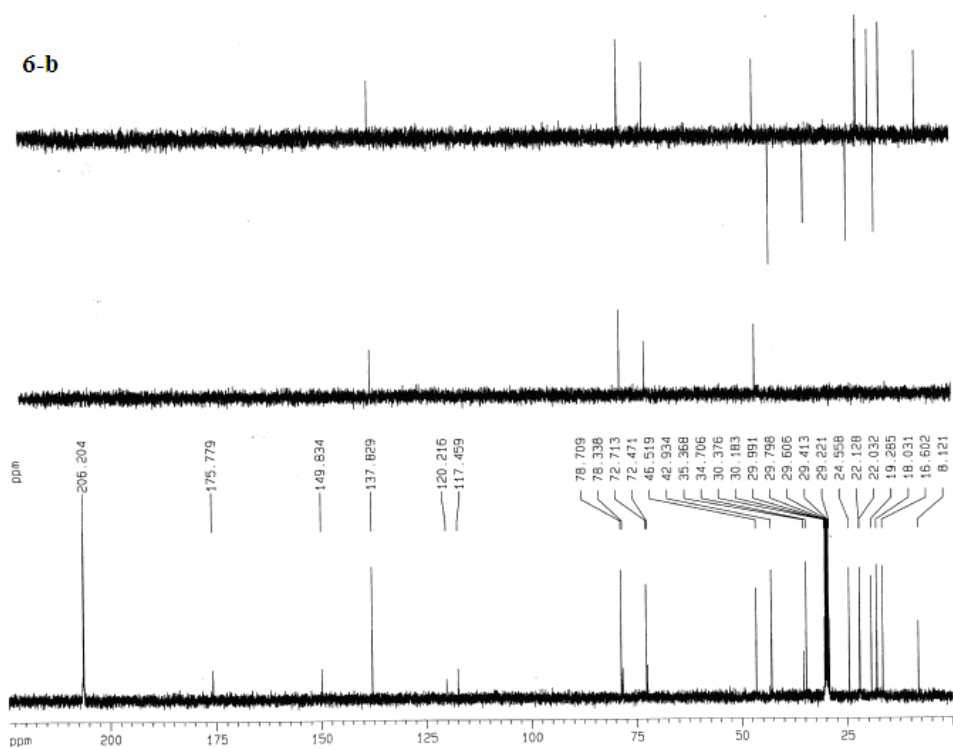


Figure S34. The  $^{13}\text{C}$  NMR of  $3\alpha$ -(2',3'-dihydroxy-2'-methylbutyryloxy)-furoepaltol (6).

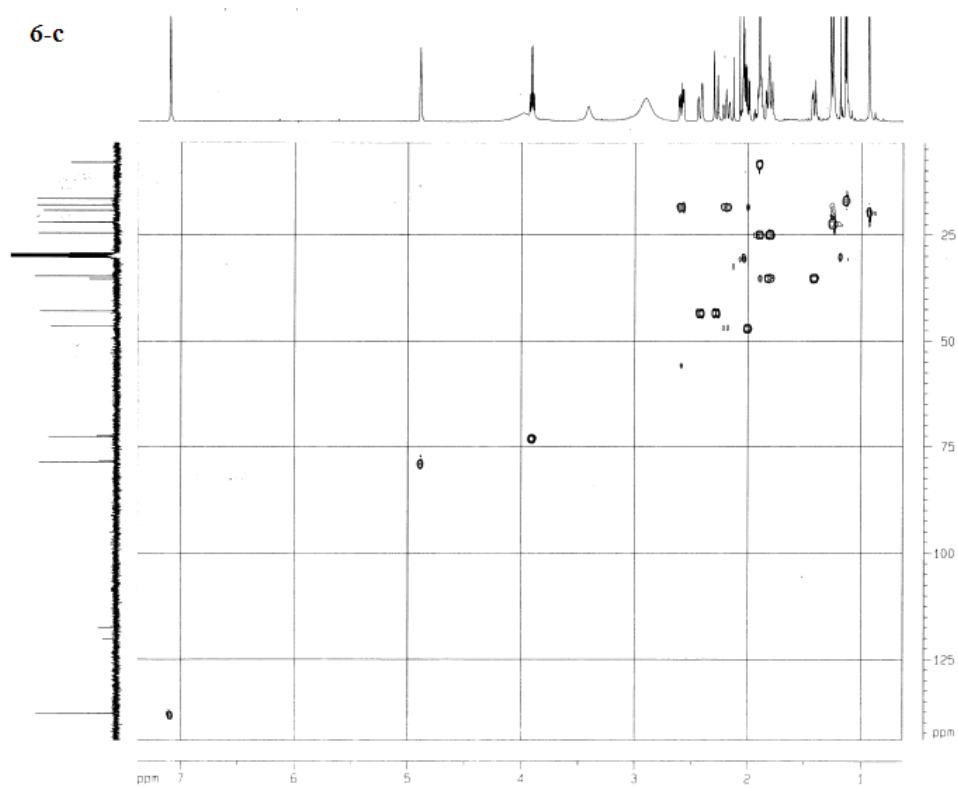
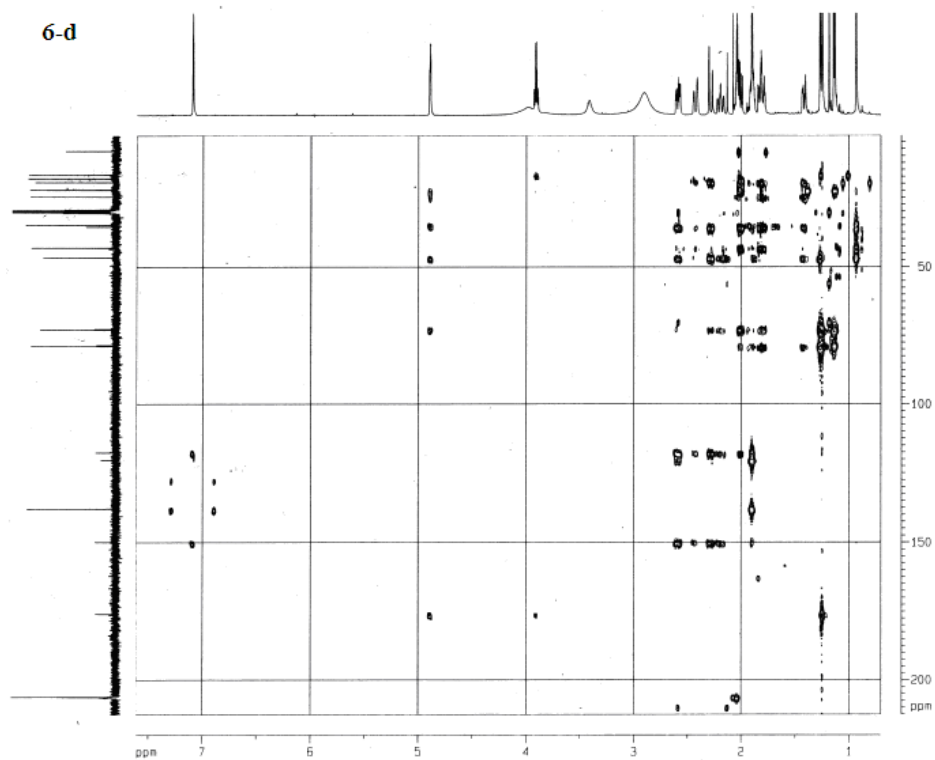
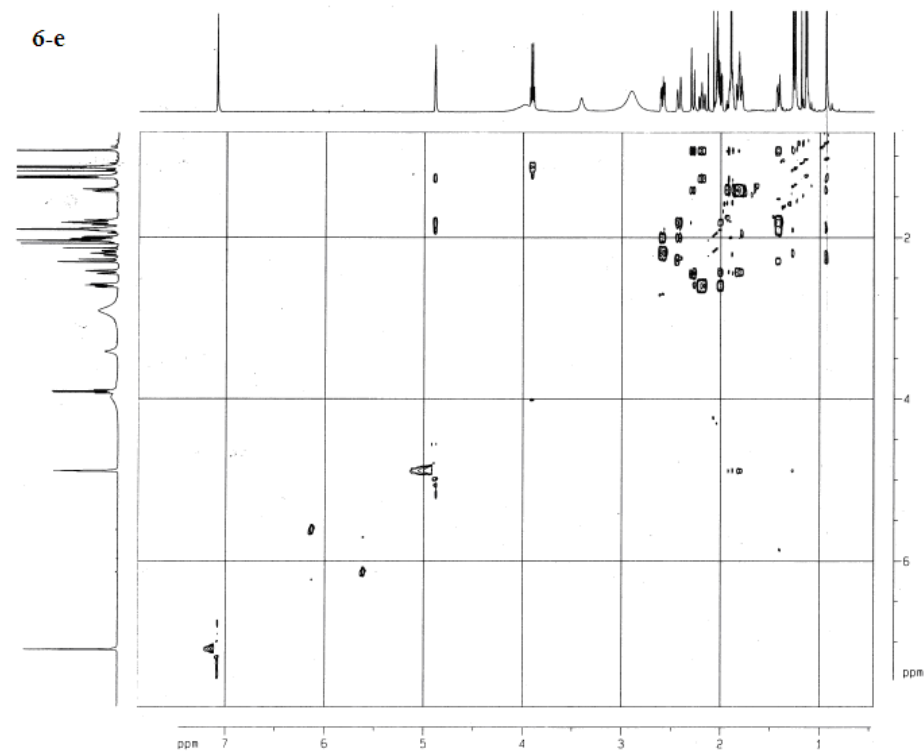


Figure S35. The HSQC of  $3\alpha$ -(2',3'-dihydroxy-2'-methylbutyryloxy)-furoepaltol (6).



**Figure S36.** The HMBC of  $3\alpha$ -(2',3'-dihydroxy-2'-methylbutyryloxy)-furoepaltol (**6**).



**Figure S37.** The ROESY of  $3\alpha$ -(2',3'-dihydroxy-2'-methylbutyryloxy)-furoepaltol (**6**).

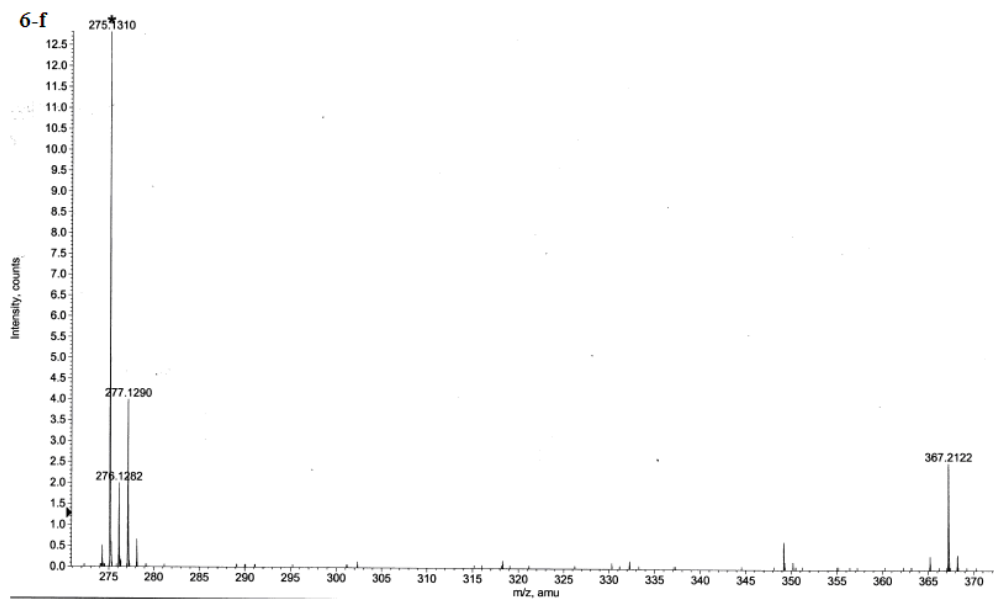


**Figure S38.** The HREIMS of  $3\alpha$ -(2',3'-dihydroxy-2'-methylbutyryloxy)-furoepaltol (**6**).

**Table S1.** Effect of the Pterodontic Acid on Aylene-Induced Ear Edema<sup>a</sup>

Group	Dose (mg/kg)	Treatment	Weight of ear (mg)	Inhibition ratio (%)
Control	20ml	ig	14.22±3.19	
Aspirin	200mg	ig	3.73±2.05**	73.7
Pterodontic acid	10 mg	ig	5.10±3.23**	64.1

<sup>a</sup> Values expressed as mean ± SD (n = 10). \*\*P<0.01 for comparison of treated groups with control.

**Table S2.** The  $^1\text{H}$  NMR Data of Those Induced Furoeudesmanes **1–6**<sup>a</sup> at 500 MHz

Position	<b>1</b>	<b>2</b>	<b>3</b>	<b>4</b>	<b>5</b>	<b>6</b>
1 $\alpha$	1.67, m	1.68, m	1.73, m	1.49, m	1.61, dt (18.0, 4.5)	1.82, br. t (13.6)
1 $\beta$	1.44, m	1.45, m	1.47, m	1.42, m	1.42, dt (18.0, 4.0)	1.42, dd (13.6, 4.0)
2 $\alpha$	1.70, m	1.90, m	1.75, m	1.80, m	1.78, m	1.82, br. t (13.6)
2 $\beta$	1.81, m	1.90, m	1.93, m	1.87, m	1.90, m	1.91, m
3 $\beta$	4.80, br. s	5.83, br. s	4.90, br. s	5.93, br. s	4.79, br. s	4.90, br. s
5 $\alpha$	1.96, dd (14.5, 5.5)	2.17, dd (15.0, 5.5)	2.00, dd (14.5, 5.5)	2.10, dd (10.5, 4.5)	1.98, dd (11.9, 4.6)	2.01, dd (12.4, 4.8)
6 $\alpha$	2.64, m	2.62, dd (19.5, 5.5)	2.64, dd (20.0, 6.0)	2.58, dd (15.5, 4.0)	2.61, dd (19.5, 5.5)	2.60, dd (15.6, 4.4)
6 $\beta$	2.23, m	2.34, m	2.22, br. t (16.5)	2.25, br. t (12.5)	2.21, br. t (18.0)	2.20, br. t (15.6)
9 $\alpha$	2.40, m	2.46, d (20.0)	2.41, d (20.5)	2.52, d (16.0)	2.40, d (15.9)	2.43, d (16.0)
9 $\beta$	2.34, m	2.32, d (20.0)	2.35, d (20.0)	2.34, d (16.0)	2.29, d (15.9)	2.29, d (16.0)
12	7.10, s	7.12, s	7.10, s	7.06, s	7.10, s	7.10, s
13	1.91, s	1.93, s	1.91, s	1.96, s	1.90, s	1.91, s
14	0.94, s	0.99, s	0.95, s	0.97, s	0.93, s	0.94, s
15	1.27, s	1.66, s	1.32, s	1.64, s	1.29, s	1.27, s
2'	5.76, s					
3'		3.04, q (5.4)	3.02, q (5.4)	5.03, q (6.3)	5.10, q (6.3)	3.92, q (6.3)
4'	1.86, s	1.25, d (5.4)	1.27, d (5.4)	1.28, d (6.3)	1.20, d (6.3)	1.14, d (6.3)
5'	2.14, s	1.48, s	1.51, s	1.31, s	1.33, s	1.25, s
4-		1.95, s		1.95, s		
OCOMe						
3'-				1.98, s	1.93, s	
OCOMe						

<sup>a</sup> Compound **4** was measured in  $\text{CDCl}_3$ , compounds **1**, **2**, **3**, **5**, and **6** in  $\text{Me}_2\text{CO}-d_6$ . *J* in Hz and  $\delta$  in ppm.

**Table S3.** The <sup>13</sup>C NMR Data of Those Induced Furoeudesmanes **1–6**<sup>a</sup> at 125 MHz

Position	<b>1</b>	<b>2</b>	<b>3</b>	<b>4</b>	<b>5</b>	<b>6</b>
1	34.9 t	33.8 t	34.8 t	32.8 t	34.5 t	34.7 t
2	24.7 t	23.6 t	24.8 t	23.2 t	24.5 t	24.6 t
3	77.0 d	74.5 d	78.7 d	74.8 d	79.6 d	78.7 d
4	72.3 s	83.9 s	72.3 s	83.4 s	72.4 s	72.5 s
5	46.9 d	45.4 d	46.5 d	44.5 d	46.5 d	46.5 d
6	18.1 t	18.5 t	18.1 t	18.0 t	18.1 t	18.0 t
7	117.6 s	117.0 s	117.5 s	115.9 s	117.4 s	117.5 s
8	149.7 s	149.5 s	149.7 s	148.8 s	149.8 s	149.8 s
9	43.1 t	43.2 t	43.2 t	42.5 t	42.9 t	42.9 t
10	35.4 s	35.4 s	35.3 s	34.7 s	35.3 s	35.4 s
11	120.2 s	120.2 s	120.2 s	119.4 s	120.1 s	120.2 s
12	137.9 d	138.2 d	137.9d	137.3d	137.9 d	137.8 d
13	8.1 q	8.1 q	8.1 q	8.1 q	8.1 q	8.1 q
14	18.1 q	19.5 q	19.3 q	18.8 q	19.2 q	19.3 q
15	22.4 q	19.0 q	22.7 q	19.4 q	22.3 q	22.1 q
1'	166.3 s	168.9 s	169.7 s	173.8 s	175.1 s	175.8 s
2'	117.3 d	60.3 s	60.3 s	75.8 s	77.1 d	78.3 s
3'	156.7 d	59.8 d	59.9 d	74.4 d	75.2 d	72.7 s
4'	27.2 q	14.1 q	14.0 q	13.1 q	13.5 q	16.6 q
5'	20.0 q	19.6 q	19.6 q	22.1 q	22.9 q	22.0 q
4-OAc		22.2 q 169.9 s		22.2 q 169.5 s		
3'-OAc				20.1 q 169.9 s	20.1 q 170.2 s	

<sup>a</sup> Compound **4** was measured in CDCl<sub>3</sub>, compounds **1**, **2**, **3**, **5**, and **6** in Me<sub>2</sub>CO-*d*<sub>6</sub>. *J* in Hz and  $\delta$  in ppm.

## References

- (S1). J. P. Ren, X. G. Wang, J. Yin, *Agricultural Sciences in China*, **2010**, *9*, 31-37.
- (S2). R. Maruthachalam, P. A. M. Mohan, S. Imran, *Nature* **2008**, *451*, 1121-1124.
- (S3). J. H. Shang, X. H. Cai, T. Feng, Y. L. Zhao, J. K. Wang, L. Y. Zhang, M. Yan, X. D. Luo, *J. Ethnopharmacol.* **2010**, *129*, 174 -181.
- (S4). (a) K. Wada, K. Munakata, *J. Agric. Food Chem.* **1968**, *16*, 471-474. (b) M. Szczepanik, R. Obara, A. Szumny, B. Gabrys, A. Halarewicz-Pacan, J. Nawrot, C. Wawrzenczyk, *J. Agric. Food Chem.* **2005**, *53*, 5905-5910.
- (S5). (a) W. L. Yee, C. T. Nick, *J. Econ. Entomol.* **1998**, *91*, 56-63. (b) L. Chen, H. H. Xu, B. L. Yin, C. Xiao, T. S. Hu, Y. L. Wu, *J. Agric. Food Chem.* **2004**, *52*, 6719-6734.
- (S6). R. Lai, H. Takeuchi, J. Jonczy, H. H. Rees, P. C. Turner, *Gene* **2004**, *342*, 243-249.
- (S7). M. Dixon, *Biochem. J.* **1953**, *55*, 170-171.
- (S8). G. V. J. Gooding, T. T. Hebert, *Phytopathology* **1967**, *57*, 1285-1287.
- (S9). Y. M. Li, L. H. Wang, S. L. Li, X. Y. Chen, Y. M. Shen, Z. K. Zhang, H. P. He, W. B. Xu, Y. L. Shu, G. D. Liang, R. X. Fang, X. J. Hao, *Proc. Nati. Acad. Sci.* **2007**, *104*, 8083-8088.
- (S10). J. Chen, X. H. Yan, J. H. Dong, P. Sang, X. Fang, Y. T. Di, Z. K. Zhang, X. J. Hao, *J. Agric. Food Chem.* **2009**, *57*, 6590-6595.
- (S11). Y. S. Wang, H. J. Fan, Y. Li, Z. L. Shi, Y. Pan, C. P. Lu, *Vaccine* **2007**, *25*, 4447-4455.
- (S12). J. Sambrook, E. Fritsch, T. Maniatis, *Molecular cloning: a laboratory manual* Cold Spring Harbor Laboratory Press, Cold Spring Harbor, NY, 1989.